

AperTO - Archivio Istituzionale Open Access dell'Università di Torino

## Charge collection efficiency degradation induced by MeV ions in semiconductor devices: Model and experiment

### This is the author's manuscript

*Original Citation:*

*Availability:*

This version is available <http://hdl.handle.net/2318/1589530> since 2016-08-26T12:04:48Z

*Published version:*

DOI:10.1016/j.nimb.2016.01.030

*Terms of use:*

Open Access

Anyone can freely access the full text of works made available as "Open Access". Works made available under a Creative Commons license can be used according to the terms and conditions of said license. Use of all other works requires consent of the right holder (author or publisher) if not exempted from copyright protection by the applicable law.

(Article begins on next page)

This Accepted Author Manuscript (AAM) is copyrighted and published by Elsevier. It is posted here by agreement between Elsevier and the University of Turin. Changes resulting from the publishing process - such as editing, corrections, structural formatting, and other quality control mechanisms - may not be reflected in this version of the text. The definitive version of the text was subsequently published in NUCLEAR INSTRUMENTS & METHODS IN PHYSICS RESEARCH. SECTION B, BEAM INTERACTIONS WITH MATERIALS AND ATOMS, 372, 2016, 10.1016/j.nimb.2016.01.030.

You may download, copy and otherwise use the AAM for non-commercial purposes provided that your license is limited by the following restrictions:

- (1) You may use this AAM for non-commercial purposes only under the terms of the CC-BY-NC-ND license.
- (2) The integrity of the work and identification of the author, copyright owner, and publisher must be preserved in any copy.
- (3) You must attribute this AAM in the following format: Creative Commons BY-NC-ND license (<http://creativecommons.org/licenses/by-nc-nd/4.0/deed.en>), 10.1016/j.nimb.2016.01.030

The publisher's version is available at:

<http://linkinghub.elsevier.com/retrieve/pii/S0168583X16000872>

When citing, please refer to the published version.

Link to this full text:

<http://hdl.handle.net/>

# Charge collection efficiency degradation induced by MeV ions in semiconductor devices: model and experiment

E. Vittone<sup>1\*</sup>, Z. Pastuovic<sup>2</sup>, M. B. H. Breese<sup>3</sup>, J. Garcia Lopez<sup>4</sup>, M. Jaksic<sup>5</sup>, J. Raisanen<sup>6</sup>, R. Siegele<sup>2</sup>, A. Simon<sup>7,8</sup>, G. Vizkelethy<sup>†9</sup>

<sup>1</sup> Department of Physics, NIS research centre and CNISM, University of Torino, via P. Giuria 1, 10125 Torino, Italy.

<sup>2</sup> Centre for Accelerator Science, (ANSTO), Locked bag 2001, Kirrawee DC NSW 2234, Australia.

<sup>3</sup> Centre for Ion Beam Applications (CIBA), Department of Physics, National University of Singapore, Singapore 117542.

<sup>4</sup> Centro Nacional de Aceleradores (CNA), Sevilla University, J. Andalucia, CSIC, Av. Thomas A. Edison 7, 41092 Sevilla, Spain.

<sup>5</sup> Department for Experimental Physics, Ruder Boškovic Institute (RBI), P.O. Box 180, 10002 Zagreb, Croatia.

<sup>6</sup> Department of Physics, University of Helsinki, Helsinki 00014, Finland.

<sup>7</sup> International Atomic Energy Agency, (IAEA) Vienna International Centre, P.O. Box 100, 1400 Vienna, Austria

<sup>8</sup> Institute of Nuclear Research of the Hungarian Academy of Sciences (ATOMKI), Debrecen, Hungary

<sup>9</sup> Sandia National Laboratories (SNL), PO Box 5800, Albuquerque, NM, USA.

**Keywords:** Charge Collection Efficiency, Silicon, Radiation damage, Ion Beam Induced Charge (IBIC), Semiconductors, MeV Ion Beams.

## Abbreviations<sup>‡</sup>

---

\* Corresponding author: ettore.vittone@unito.it

† Sandia National Laboratories is a multi-program laboratory managed and operated by Sandia Corporation, a wholly owned subsidiary of Lockheed Martin Corporation, for the U.S. Department of Energy's National Nuclear Security Administration under contract DE-AC04-94AL85000.

‡ DIB: Damaging Ion Beam; PIB: Probing Ion Beam; IBIC: Ion Beam Induced Charge; NIEL: Non-Ionizing Energy Loss; CCE Charge Collection Efficiency

## Abstract

This paper investigates both theoretically and experimentally the charge collection efficiency (CCE) degradation in silicon diodes induced by energetic ions. Ion beam induced charge (IBIC) measurements carried out on n- and p-type silicon diodes which were previously irradiated with MeV He ions show evidence that the CCE degradation doesn't only depend on the mass, energy and fluence of the damaging ion, but also depends on the ion probe specie and on the polarization state of the device. A general one-dimensional model is derived, which accounts for the ion-induced defect distribution, the ionization profile of the probing ion and the charge induction mechanism. Using the ionizing and non-ionizing energy loss profiles resulting from simulations based on the binary collision approximation and on the electrostatic/transport parameters of the diode under study as input, the model is able to accurately reproduce the experimental CCE degradation curves without introducing any phenomenological additional term or formula. Although limited to low level of damage, the model is quite general, including the displacement damage approach as a special case and can be applied to any semiconductor device. It provides a method to measure the capture coefficients of the radiation induced recombination centres. They can be considered indexes, which can contribute to assessing the relative radiation hardness of semiconductor materials.

## 1. Introduction

While the effect of radiation induced defects on the properties of semiconducting and insulating materials and devices has been studied for many years, there are still significant gaps in the understanding of what types of defects are formed, how they can be detected and their effects on electrical and structural properties. This study is based on research conducted within an IAEA Coordinated Research Project (CRP, reference F11016 [1]). The main objective of this project was the enhancement of the understanding of which types of defects are created by high energy ion irradiation and what are their effects on electronic properties of semiconductors and insulators. A further objective is to develop means of defining and measuring radiation resistance of materials, with the ultimate aim of thereby improving it. This involves defining an experimental protocol to determine the key parameters for characterization of the effects of radiation damage on semiconductor materials and devices. Here we focus on the modified electronic properties of silicon, as being the most important and the most widely-studied semiconductor [2]. In Float Zone (FZ) silicon where the oxygen content is low ( $< 10^{16} \text{ cm}^{-3}$ ), the defect spectrum produced after ion irradiation and without any annealing is

1  
2  
3  
4 relatively straightforward; the main effect is the creation of acceptor-like defect complexes, which, in  
5  
6 n-type silicon can cause inversion to p-doping at very high fluences. After high fluence proton  
7  
8 irradiation of n-type silicon, at the ion end-of-range where these defects overlap with the implanted  
9  
10 hydrogen, hydrogen-related donors are formed which again cause inversion to n-doping [3]. In  
11  
12 Czochralski (CZ) silicon a host of oxygen-related doping effects can occur due to the higher oxygen  
13  
14 concentration (up to  $10^{18} \text{ cm}^{-3}$ ) [2]. The defect profile produced by ion irradiation of silicon thus  
15  
16 depends on many factors, including ion type, fluence, oxygen and other impurity concentrations of the  
17  
18 wafer and annealing conditions, if any.

19 We confine our study to the low fluence ion irradiation of FZ silicon, so that the defects produced do  
20  
21 not significantly alter the basic device properties such as doping density and thereby modify the  
22  
23 electrostatic fields present. We do not investigate any high temperature annealing treatment performed  
24  
25 after irradiation.

26 The experimental protocol, proposed in a previous paper [4], consists of two steps: the former is the  
27  
28 controlled irradiation of the device under study by focused light MeV ions beams (in the following  
29  
30 named DIBs: damaging ion beams), which induce defects in selected areas (typically of  $100 \times 100 \mu\text{m}^2$ )  
31  
32 at different fluences. This methodology allows the use of ions with different masses and energies to  
33  
34 generate damage profiles of different densities in the same sample. Since the characterization phase is  
35  
36 carried out a few days (during which the sample is kept at room temperature) after irradiation, only  
37  
38 permanent damage induced by the displacement of atomic nuclei will be considered.

39 The second step is the characterization of the effects that ion irradiation induces on the electronic  
40  
41 properties of the semiconductor device under study. Here, we consider the charge collection efficiency  
42  
43 (CCE) degradation as a function of DIB fluence an appropriate observable to evaluate the radiation  
44  
45 hardness of the device. The characterization method used here is Ion Beam Induced Charge (IBIC)  
46  
47 microscopy [5] in which the number of charge carriers produced by each ion within a focused ion beam  
48  
49 (in the following named PIBs: probing ion beams) of a few thousand ions per second is detected. This  
50  
51 approach is well-suited here, as the same experimental geometry, and frequently the same ions, are  
52  
53 used both to damage the material under investigation and also to detect the effects of damage by the  
54  
55 reduced charge pulse height produced by each subsequent ion. Moreover, the analytical potential of this  
56  
57 experimental methodology is further enhanced by the possibility of measuring the CCE degradation in  
58  
59 different polarization conditions of the device under study.

60 In order to fully exploit the wealth of information contained in the combination of the CCE  
61  
62 degradation curves obtained in different experimental conditions, a model is required which accounts  
63  
64  
65

for the atom displacements produced by the ion/atom interaction during the damage step, for the generation profiles of carriers produced by PIBs and for the charge induction mechanism in the semiconductor device.

In this paper, we propose a model which integrates the ionization and non-ionization ion energy loss in solids, the theory of charge induction in semiconductors [5][6] and the electron/hole generation-recombination model of Shockley-Read-Hall [7]. We have used the computer code SRIM [8] to calculate the Bragg curve and the vacancy profile, respectively. The former provides the source term of a set of differential equations, which describe the charge induced at the sensing electrode by the motion of the free carriers generated by ionization. The latter allows the recombination term in the semiconductor continuity equation to be expressed in terms of displacement damage, which is assumed to be proportional to the distribution of primary point defects acting as recombination centres and hence affecting the carrier lifetimes.

In the case of full depletion conditions, the model provides an analytical expression, which is effective to fit the experimental CCE degradation as function of DIB fluence and measured using different PIBs in different diode polarization conditions. The fitting parameters are the capture coefficients of the radiation induced recombination centres, which can be considered the key parameters for determining the effective radiation hardness of a material.

## 2. Theory

The model takes following processes into account:

- i) The final depth profile of the defect distribution formed by primary ions and recoils;
- ii) The nature of the ion probe interaction with the partly-damaged detector (device);
- iii) The charge collection mechanism of free carriers generated by the probing ions, which depends on the electrostatics of the device.

All these processes can be integrated into a unique model based on the theory of the IBIC technique [9][10].

The basic assumption for the validity of our model is the “quasi-steady state approximation” [11]: free charge carriers generated by the single ion probe interaction with the semiconductor material do not significantly perturb the electrostatic field within the tested device. This assumption is equivalent to the statement that free carriers, electrons (n) and holes (p), generated by ionization, move in a static electric field given by the solution of the steady state basic equations of semiconductors. The total

induced charge  $Q_s(t)$  is then given by the superposition of the individual electron and hole contributions, i.e.

$$(1) \quad Q_s(t) = \int_{\Omega} d^3\rho [Q_n(t; \vec{\rho}) + Q_p(t; \vec{\rho})] \cdot \Gamma(\vec{\rho})$$

where  $Q_n$ ,  $Q_p$  are the induced charge at the sensitive electrode (S) induced by the motion of electrons and holes, respectively;  $\Omega$  is the active volume of the device and  $\Gamma$  is the generation profile distribution.

By virtue of the quasi-steady state approximation, no interaction between excess charge carriers is taken into account, i.e. we assume the plasma and/or high charge injection effects are negligible. As a consequence, this approximation allows decoupling of the electrostatics (Poisson's equation) and the carrier continuity equations. It follows that the  $Q_n, Q_p$  terms in (1) can be considered as the sum of the individual contributions of electrons/holes moving separately within the static electric field region.

The instantaneous current ( $i_s$ ) induced at the sensitive electrode by the motion of an elementary charge  $q$  with a drift velocity  $\vec{v}$  can be calculated by means of a general formula, introduced by J.B. Gunn [13] [14]:

$$(2) \quad i_s = -q \cdot \vec{v} \cdot \frac{\partial \vec{F}}{\partial V_s}$$

$\frac{\partial \vec{F}}{\partial V_s}$  is "Gunn's weighting field", which is defined as the partial derivative of the actual electric field ( $\vec{F}$ ) with respect to the bias voltage  $V_s$  applied to the sensing electrode, while the voltage is kept constant on all the other electrodes.

The time integral of eq. (2) gives the charge  $q_s(t; \vec{\rho})$  induced at the sensing electrode at time  $t$  by a charge  $q$  generated at  $t=0$  in a position  $\vec{r} = \vec{\rho}$  :

$$(3) \quad q_s(t; \vec{\rho}) = \int_0^t dt' i_s(t') = -q \cdot \int_0^t dt' \left[ \vec{v} \cdot \frac{\partial \vec{F}}{\partial V_s} \right] = -q \cdot \int_{\vec{\rho}}^{r(t)} \frac{\partial \vec{F}}{\partial V_s} \cdot d\vec{\ell} = q \cdot \left[ \frac{\partial \psi}{\partial V_s} \Big|_{r(t)} - \frac{\partial \psi}{\partial V_s} \Big|_{\vec{\rho}} \right]$$

where  $\psi$  is the actual electrostatic potential (i.e.  $\vec{F} = -\nabla\psi$ ),  $r(t)$  is the position of the moving charge at time  $t$ , and the line integral is calculated along the carrier trajectory. The induced charge in the case of a moving single point charge is then simply given by the difference of the "Gunn's weighting

potential”  $\left( \frac{\partial \psi}{\partial V_s} \right)$  between the final and initial positions of the point charge. A method to calculate the weighting field is given in [15].

The total charge  $Q_s$  induced at the sensing electrode at time  $t$  by the motion of free carriers generated in a certain position  $\bar{\rho}$ , is obtained by combining Eq.(3) with Eq. (1):

$$(4) \quad Q_s(t; \bar{\rho}) = Q_n(t; \bar{\rho}) + Q_p(t; \bar{\rho}) = -q \cdot \int_0^t dt' \int_{\Omega} d^3r \left[ n(\bar{r}, t'; \bar{\rho}) \cdot \bar{v}_n(\bar{r}) + p(\bar{r}, t'; \bar{\rho}) \cdot \bar{v}_p(\bar{r}) \right] \cdot \frac{\partial \bar{F}(\bar{r})}{\partial V_s} \Bigg|$$

where  $n$  and  $p$  are the excess charge concentrations of electrons and holes, respectively, whose spatial-temporal evolution can be calculated by solving the electron/hole continuity equations [11] [16], with the initial conditions:  $n(\bar{r}, t = 0; \bar{\rho}) = p(\bar{r}, t = 0; \bar{\rho}) = \delta(\bar{r} - \bar{\rho})$ , where  $\delta$  is the Dirac delta function.

It is important to understand that decoupling of the electron and hole contributions in Eq. (1) implies not only the negligible interaction of electrons and holes, but also the linear superposition of the electron/hole recombination/trapping processes.

As a consequence the electron/hole continuity equations contain only linear terms and the “adjoint model”, proposed by T.H. Prettyman [9][10] [11][12] can be effectively adopted.

Actually, if the free carrier generation terms are defined in the following manner [17]

$$(5) \quad \begin{aligned} G_n(\bar{r}) &= +\bar{v}_n(\bar{r}) \cdot \frac{\partial \bar{F}(\bar{r})}{\partial V_s} - \nabla \left[ D_n \cdot \frac{\partial \bar{F}(\bar{r})}{\partial V} \right] \\ G_p(\bar{r}) &= +\bar{v}_p(\bar{r}) \cdot \frac{\partial \bar{F}(\bar{r})}{\partial V_s} + \nabla \left[ D_p \cdot \frac{\partial \bar{F}(\bar{r})}{\partial V} \right] \end{aligned}$$

two terms in eq. (4) are the Green’s function of the carrier (electron or hole) continuity equations.

As a consequence, the contribution of electrons and holes to the induced charge can be evaluated by solving the adjoint equations of the relevant continuity equations, i.e.

$$(6) \quad \frac{\partial \xi^+}{\partial t} = (-1)^{(\alpha+1)} \cdot \bar{v}_\xi \cdot \bar{\nabla} \xi^+ + \nabla (D_\xi \cdot \bar{\nabla} \xi^+) - R_\xi + G_{\xi,s}^+$$

where  $\xi^+$  is the adjoint function for electrons ( $\xi^+ = n^+; \alpha=0$ ) and for holes ( $\xi^+ = p^+; \alpha=1$ ),  $D_{n,p}$  is the electron or hole diffusion coefficient and  $R_\xi$  is the linearized recombination term. Assuming homogeneous boundary and initial conditions, it can be demonstrated [11] that the charge at the sensitive electrode induced by the motion of free carriers generated at the starting point  $\bar{\rho}$  is given by:



$$(7) \quad Q_{n,p}(t; \vec{\rho}) = q \cdot (n^+(\vec{\rho}, t) + p^+(\vec{\rho}, t))$$

The recombination term  $R_{n,p}$  in eq. (6) can be linearized if

- iv) the excess free carrier concentration is small compared to the number of available recombination centres.
- v) the de-trapping time is small compared to the carrier transit time from any generation point to the collecting electrode.

In this case,  $R_{n,p}$  is proportional to the carrier concentration, i.e.

$$(8) \quad R_n = \frac{n}{\tau_n}; \quad R_p = \frac{p}{\tau_p}$$

where  $\tau_{n,p}$  is the electron and hole lifetime, respectively.

According to the Shockley-Read-Hall model, the carrier lifetime is related to the concentration of recombination centres  $N^T$  through the following expression [7][18]:

$$(9) \quad \frac{1}{\tau_{n,p}} = N_{n,p}^T \cdot \sigma_{n,p} \cdot v_{n,p}^{th}$$

where  $v_{n,p}^{th}$  and  $\sigma_{n,p}$  are the carrier thermal velocities and the carrier capture cross sections, respectively.

Eq. (9) allows the effect of radiation damage to be integrated in the unique radiation damage model by assuming

- vi) the proportionality of the recombination centre concentration  $N^T$  and the concentration of vacancy-interstitial Frenkel pairs as created immediately after irradiation as can be calculated from Binary Collision Approximation codes, such as SRIM [8] or Marlowe [19].

It follows that the carrier lifetime distributions can be related to the recombination parameters using the following equation [2][20]:

$$(10) \quad \frac{1}{\tau_{n,p}(\vec{r})} = N_{n,p}^{T0} \cdot \sigma_{n,p}^0 \cdot v_{n,p}^{th} + N_{n,p}^T(\vec{r}) \cdot \sigma_{n,p} \cdot v_{n,p}^{th} = \frac{1}{\tau_{n,p}^0} + K_{n,p}(\vec{r}) \cdot \Phi$$

where the superscript “0” denotes terms corresponding to the pristine material ( $\tau_{n,p}^0$  is assumed constant),  $\tau_{n,p}$  is the lifetime after the irradiation with the fluence  $\Phi$  of damaging ions, which generate the concentration  $N^T(\vec{r})$  of recombination centres with capture cross section  $\sigma_{n,p}$ ;  $K_{n,p}$  is the (recombination) lifetime damage coefficient defined as

$$(11) \quad K_{n,p}(\vec{r}) = \frac{N_{n,p}^T(\vec{r}) \cdot \sigma_{n,p} \cdot v_{n,p}^{th}}{\Phi}$$

Furthermore, under the previous assumption of  $N^T$  and Frenkel pairs proportionality, the concentration of active recombination centres  $N_{n,p}^T$  scales with the damaging ion fluence  $\Phi$ . The proportionality factor is given by the product of the vacancy concentration distribution per ion, i.e. the vacancy distribution profile  $V(\vec{r})$  (which can be calculated by the SRIM [8] or Marlowe [19] codes), and the average number of active defects (carrier traps) generated by a single vacancy  $k$ :

$$(12) \quad N_{n,p}^T(\vec{r}) = k_{n,p} \cdot V(\vec{r}) \cdot \Phi \Rightarrow K_{n,p}(\vec{r}) = k_{n,p} \cdot V(\vec{r}) \cdot \sigma_{n,p} \cdot v_{n,p}^{th}.$$

In the studied case of a semiconductor device with a planar geometry, we can further simplify the problem by reducing it to only one dimension (depth), which can be realized by considering the normal irradiation of the front contact electrode and by assuming the trajectories of high energy ion projectiles (MeV energy range) in a material are nearly straight lines, i.e. the end of an ion range is much larger than the lateral straggling of a light ion producing Frenkel pairs directly. Moreover, using a raster-scanned ion microbeam with micrometre spatial resolution for the vacancy production (ion projectiles entering the surface of a device within a pixel of  $1\mu\text{m}$  by  $1\mu\text{m}$  size with maximum angular deviation from normal incidence  $\pm 1^\circ$ ), the vacancy distribution generated along the ion cascade by secondary recoils deviating from the straight line direction of the projectile is averaged. It is important that due to irradiation conditions with the average ion beam rate up to 10 kHz and the pixel dwell time of 500  $\mu\text{s}$ , we can assume that defects formed in the individual cascades are well separated both in time and spatially. The cumulative effect of multiple scanning the region of interest to create each damage structure (usually  $100 \times 100 \mu\text{m}^2$ ) is the uniform cross sectional areal distribution of finally formed defects.

As a consequence, we need to consider the generation of vacancies occurring mainly along the ion track, which develops along the direction normal to the irradiated electrode (i.e. x-direction).

As above described, the IBIC technique was used to measure the CCE degradation. Therefore, the carrier generation volume, which is nearly cylindrical with a diameter of tens of nanometres [5], can be assumed as a function only of the x coordinate and proportional to the ionization energy loss profile:

$$(13) \quad \frac{dE_I}{dx} = \Gamma(x) \cdot \varepsilon_{np}$$

where  $\varepsilon_{np}$  is the average energy required to create electron/hole pairs (in silicon 3.6 eV [21]),  $E_I$  is the energy and  $\frac{dE_I}{dx}$  is the ionization energy loss of the ion probe.

Moreover, if we consider that in our experimental conditions all carrier generation and recombination processes occur within the depletion region of a device, the dominant charge transport mechanism is the carrier drift caused by the applied electric field whose direction is perpendicular to the electrodes. As a consequence of the carrier generation, transport and recombination occurs only within the depleted region, the diffusion of charge carriers is reasonably assumed to be negligible and the “Gunn’s weighting potential” assumes a form of the conventional weighting potential as defined by the “Shockley-Ramo” theorem [22][23][24][25].

In the following, we will consider only the one-dimensional geometry outlined in Fig. 1a. The cathode is located at  $x=0$  and the anode located at  $x=d$  is grounded.

In these conditions the adjoint equations (6) can be re-written as the following first order space-time differential equations:

$$(14) \quad \begin{cases} \frac{\partial n^+(x, t)}{\partial t} = -v_n(x) \cdot \frac{\partial n^+(x, t)}{\partial x} - n^+(x, t) \cdot \left( \frac{1}{\tau_n^0} + k_n \cdot V(x) \cdot \sigma_n \cdot v_n^{th} \right) + v_n(x) \cdot \frac{\partial F(x)}{\partial V_s}; \\ \frac{\partial p^+(x, t)}{\partial t} = +v_p(x) \cdot \frac{\partial p^+(x, t)}{\partial x} - p^+(x, t) \cdot \left( \frac{1}{\tau_p^0} + k_p \cdot V(x) \cdot \sigma_p \cdot v_p^{th} \right) + v_p(x) \cdot \frac{\partial F(x)}{\partial V_s}; \end{cases}$$

with homogeneous initial ( $t=0$ ) and boundary conditions defined at the irradiated (at  $x=0$ ) and back (at  $x=d$ ) electrodes:

$$(15) \quad \begin{cases} n^+(x=d, t) = n^+(x=0, t) = n^+(x, t=0) = 0 \\ p^+(x=d, t) = p^+(x=0, t) = p^+(x, t=0) = 0 \end{cases}$$

Usually the total induced charge is considered in the experiment, so the time dependent adjoint equations (14) asymptotically converge to the following steady state equations:

$$(16) \quad \begin{cases} v_n(x) \cdot \frac{dn^+(x)}{dx} = -n^+(x) \cdot \left( \frac{1}{\tau_n^0} + k_n \cdot V(x) \cdot \sigma_n \cdot v_n^{th} \right) + v_n(x) \cdot \frac{\partial F(x)}{\partial V_s}; \\ -v_p(x) \cdot \frac{dp^+(x)}{dx} = -p^+(x) \cdot \left( \frac{1}{\tau_p^0} + k_p \cdot V(x) \cdot \sigma_p \cdot v_p^{th} \right) + v_p(x) \cdot \frac{\partial F(x)}{\partial V_s}; \end{cases}$$

with the following boundary conditions:

$$(17) \quad \begin{cases} n^+(x=d)=0 \\ p^+(x=0)=0 \end{cases}$$

their solution is given by the following expressions:

$$(18) \quad \begin{cases} n^+(x) = \int_x^d dy \cdot \frac{\partial F(y)}{\partial V_s} \cdot \exp \left[ - \int_x^y dz \left( \frac{1}{v_n(z) \cdot \tau_n^0} + \Phi \frac{k_n \cdot V(z) \cdot \sigma_n \cdot v_n^{th}}{v_n(z)} \right) \right]; \\ p^+(x) = \int_0^x dy \cdot \frac{\partial F(y)}{\partial V_s} \cdot \exp \left[ - \int_y^x dz \left( \frac{1}{v_p(z) \cdot \tau_p^0} + \Phi \frac{k_p \cdot V(z) \cdot \sigma_p \cdot v_p^{th}}{v_p(z)} \right) \right]; \end{cases}$$

In conclusion, the solution of the steady state equations (16), integrated in eq. (1) provides the following expression of the charge collected at the sensitive electrode:

$$(19) \quad Q_s = q \cdot \int_0^d dx \cdot \Gamma(x) \left\{ \int_x^d dy \cdot \frac{\partial F(y)}{\partial V_s} \cdot \exp \left[ - \int_x^y dz \left( \frac{1}{v_n(z) \cdot \tau_n^0} + \Phi \frac{k_n \cdot V(z) \cdot \sigma_n \cdot v_n^{th}}{v_n(z)} \right) \right] + \int_0^x dy \cdot \frac{\partial F(y)}{\partial V_s} \cdot \exp \left[ - \int_y^x dz \left( \frac{1}{v_p(z) \cdot \tau_p^0} + \Phi \frac{k_p \cdot V(z) \cdot \sigma_p \cdot v_p^{th}}{v_p(z)} \right) \right] \right\}$$

Eq. (19) is a general expression, whose validity stems from the assumption of low radiation damage, which is described by the linearized recombination terms given by eqs. (8) to (12).

Finally, normalizing  $Q_s$  by the charge induced in the pristine sample  $Q_0$ , the expression for the charge collection efficiency as a function of the DIBs fluence  $\Phi$  is:

$$(20) \quad CCE = \int_0^d dx \cdot \gamma(x) \left\{ \int_x^d dy \cdot \frac{\partial F(y)}{\partial V_s} \cdot \exp \left[ - \int_x^y \frac{dz}{\lambda_n(z)} \right] + \int_0^x dy \cdot \frac{\partial F(y)}{\partial V_s} \cdot \exp \left[ - \int_y^x \frac{dz}{\lambda_p(z)} \right] \right\}$$

where we have assumed that the induced charge is totally collected in the pristine device,

$$(21) \quad \gamma(x) = \frac{1}{E_I} \cdot \frac{dE_I}{dx}$$

is the normalized ionization energy loss profile and  $\lambda$  is the mean free path (drift length) of carriers:

$$(22) \quad \frac{1}{\lambda_{n,p}(x)} = \frac{1}{\lambda_{n,p}^0(x)} + \Phi \cdot \alpha_{n,p} \cdot \frac{V(x)}{v_{n,p}(x)}$$

where  $\lambda_{n,p}^0(x) = v_{n,p}(x) \cdot \tau_{n,p}^0$  is the carrier drift length in the pristine material, which is assumed to be much longer than  $d$  and

$$(23) \quad \alpha_{n,p} = k_{n,p} \cdot \sigma_{n,p} \cdot v_{n,p}^{th}$$

are the capture coefficients, as usually defined in the Shockley-Read-Hall model [7].

Borrowing the basic concepts from the scattering theory [26], the integrands at the exponent of the nested integrals in eq. (20) have the meaning of the probability  $P_{n,p}$  that a carrier will be stopped in a slab of infinitesimal thickness  $dx$ :

$$(24) \quad P_{n,p}(x) \cdot dx = \frac{dx}{\lambda_{n,p}(x)} = \rho_{n,p}(x) \cdot \sigma_{n,p}^{\text{eff}}(x) \cdot dx = [\Phi \cdot k_{n,p} \cdot V(x)] \cdot \left( \sigma_{n,p} \frac{v_{n,p}^{\text{th}}}{v_{n,p}(x)} \right) \cdot dx$$

where  $\rho(x) = \Phi \cdot k_{n,p} \cdot V(x)$  is the density of recombination centres of effective cross section

$$(25) \quad \sigma_{n,p}^{\text{eff}}(x) = \left( \sigma_{n,p} \frac{v_{n,p}^{\text{th}}}{v_{n,p}(x)} \right)$$

present in the slab.

It is worth noticing that  $\sigma_{n,p}^{\text{eff}}$  is inversely proportional to the carrier drift velocity, i.e. it decreases as the velocity increases. This conclusion resembles the  $(1/v)$  law relevant to the neutron capture by a free nucleus (if the complex scattering length for neutron-nucleus interaction is constant) [26] and its simple interpretation can be adopted: as the carrier velocity decreases, the carrier lingers for a longer time in the neighbourhood of the recombination centre, which has a longer time to capture a charge carrier.

Although Eq. (20) provides the solution of the CCE degradation problem, its complex analytical expression can obscure its physical meaning. In the following we will discuss briefly some more transparent cases which are routinely used.

## 2.I. Case I: derivation of the Hecht's formula.

The Hecht's formula describes the charge collection efficiency in a simple planar semiconducting device in following conditions:

I) A constant vacancy profile throughout the entire device:  $V(x) = \frac{V_T}{d}$ , where  $V_T$  is the total number of vacancies generated by a single damaging ion within the active volume

II) Full depletion conditions:  $\frac{\partial F}{\partial V_s} = \frac{1}{d}$

III) Constant carrier velocity profiles:  $v_{n,p}(x) = v_{n,p} \Rightarrow \sigma_{n,p}^{\text{eff}} = \left( \sigma_{n,p} \frac{v_{n,p}^{\text{th}}}{v_{n,p}} \right)$

These conditions can be, for example, met in p-i-n junction diodes working at sufficiently high applied reverse bias, in order to generate an almost uniform electric field and, then, a constant velocity field profile, or, as a first approximation, in solid state ionization chambers (e.g. CdTe or diamond radiation detectors [5]).

Under these conditions, the solution of eq. (20) is:

$$(26) \quad CCE = \int_0^d dx \cdot \gamma(x) \left\{ \frac{\lambda_n}{d} \cdot \left[ 1 - \exp\left(-\frac{d-x}{\lambda_n}\right) \right] + \frac{\lambda_p}{d} \cdot \left[ 1 - \exp\left(-\frac{x}{\lambda_p}\right) \right] \right\}$$

which is the generalized Hecht's equation [25]. If the generation occurs at the cathode ( $x=0$ ), i.e.  $\gamma(x) = \delta(x)$ , the charge collected at the sensing electrode originates only from one carrier type (electrons) and eq. (26) converges to the conventional Hecht's equation. It is worth noticing that, in this particular case, the drift length is a decreasing function of the DIBs fluence:

$$(27) \quad \lambda_n = v_n \cdot \left( \frac{\tau_n^0}{1 + \Phi \cdot k_n \cdot \frac{V_T \cdot \sigma_n \cdot v_n^{th}}{d} \cdot \tau_n^0} \right)$$

## 2.II. Case II: low level of damage.

In this case, we assume the low level of damage in a pristine ideal device and the drift length being much longer than the extent of the depletion region (i.e.  $\lambda_{n,p} > \lambda_{n,p}^0 \gg d$ ). Under these approximations, the exponentials in eq. (20) can be expanded in Taylor series, providing the following approximated expression:

$$(28) \quad \begin{aligned} CCE &\cong \int_0^d dx \cdot \gamma(x) \left\{ \int_x^d dy \cdot \frac{\partial F(y)}{\partial V_s} \cdot \left[ 1 - \int_x^y \frac{dz}{\lambda_n(z)} \right] + \int_0^x dy \cdot \frac{\partial F(y)}{\partial V_s} \cdot \left[ 1 - \int_y^x \frac{dz}{\lambda_p(z)} \right] \right\} = \\ &= 1 - \Phi \cdot \int_0^d dz \cdot V(z) \cdot \left\{ k_n \cdot \sigma_n^{eff}(z) \cdot \int_z^d dy \cdot \frac{\partial F(y)}{\partial V_s} \cdot \int_0^z dx \cdot \gamma(x) + k_p \cdot \sigma_p^{eff}(z) \cdot \int_0^z dy \cdot \frac{\partial F(y)}{\partial V_s} \cdot \int_z^d dx \cdot \gamma(x) \right\} \end{aligned}$$

Being, by definition,

$$(29) \quad \int_0^d dx \cdot \gamma(x) = \int_0^d dx \cdot \frac{\partial F(x)}{\partial V_s} = 1.$$

Equation (28) provides the evidence for different roles played by the two carriers. To simplify, let us consider a vacancy profile localized at  $x=x_0$ , i.e.  $V(x) = V_0 \cdot \delta(x-x_0)$ . If the generation profile extinguishes

at a depth  $x < x_0$ , i.e.  $\gamma(x) = \theta(x_0 - x)$ , where  $\theta$  is the Heaviside step function, it is apparent that only electrons, travelling from 0 to  $d$ , cross the damaged region and might suffer recombination, whereas the contribution of holes, moving in the opposite direction, is null. This situation is summarized in Fig. 1b, which shows the scheme of a  $p^+/n/n^+$  junction diode, which is damaged with DIBs, which induce a vacancy profile  $V(x)$  peaked more deeply than the generation profile  $\gamma(x)$ .

This simple consideration provides the basis of the experimental protocol developed in the following section, which allows the recombination/trapping of both types of charge carriers (electrons and holes), that contribute to the CCE degradation, to be discriminated.

### 2.III. Case III: derivation of the Non Ionizing Energy Loss (NIEL) displacement damage formula

Starting from eq. (28), and assuming the constant vacancy profile up to a depth  $R < d$  (i.e.  $V(z) = \theta(R - z) \cdot \frac{V_T}{R}$ , where  $V_T$  is the total number of vacancies), the linear degradation of CCE can be expressed as follows:

$$(30) \quad CCE \cong 1 - \Phi \cdot \frac{V_T}{R} \cdot \int_0^R dz \cdot \left\{ k_n \cdot \sigma_n^{\text{eff}}(z) \cdot \int_z^d dy \cdot \frac{\partial F(y)}{\partial V_S} \cdot \int_0^z dx \cdot \gamma(x) + k_p \cdot \sigma_p^{\text{eff}}(z) \cdot \int_0^z dy \cdot \frac{\partial F(y)}{\partial V_S} \cdot \int_z^d dx \cdot \gamma(x) \right\}$$

This expression can be connected to the phenomenological concept of “displacement damage dose”  $D_d$  proposed by Messenger et al. [27][28][29]. The displacement damage dose is defined as the displacement damage energy deposition per unit mass of material and can be calculated as the product of the particle fluence and the respective NIEL of the particle. The NIEL value is an estimate of the rate of energy loss due to atomic displacements as the particle traverses a material. In the framework of the NIEL theory, the CCE decreases with the accumulated displacement damage dose ( $D_d$ ) through the following simple expression:

$$(31) \quad CCE = 1 - K_{\text{ed}} \cdot D_d$$

where  $K_{\text{ed}}$  is the equivalent damage factor defining the rate of linear decrease. The displacement damage dose  $D_d$  is defined as follows:

$$(32) \quad D_d = \left( \frac{M}{\rho} \cdot \frac{V_T \cdot \Phi}{R} \right)$$

where  $M$  is the average defect production energy deposited through atomic displacement ( $M=54.5$  eV in Si using the modified Kinchin-Pease formula) and  $\rho$  ( $=2.32 \text{ g}\cdot\text{cm}^{-3}$ ) is the mass density of the irradiated material [27]. The units of  $D_d$  are typically  $\text{eV}\cdot\text{cm}^2\cdot\text{g}^{-1}$ .

By comparing eqs. (30) - (32), we obtain the following analytical expression for the equivalent damage factor:

$$(33) \quad K_{ed} = \frac{\rho}{M} \cdot \int_0^R dz \cdot \left\{ k_n \cdot \sigma_n^{eff}(z) \cdot \int_z^d dy \cdot \frac{\partial F(y)}{\partial V_s} \cdot \int_0^z dx \cdot \gamma(x) + k_p \cdot \sigma_p^{eff}(z) \cdot \int_0^z dy \cdot \frac{\partial F(y)}{\partial V_s} \cdot \int_z^d dx \cdot \gamma(x) \right\}$$

This expression explicitly shows the dependence of the equivalent damage factor  $K_{ed}$  on: a) the electrostatics of the device, b) the carrier transport and recombination features and c) the ion probe ionization profiles, summarized by the terms  $(k_{n,p} \cdot \sigma_{n,p}^{eff})$ ,  $\frac{\partial F}{\partial V_s}$  and  $\gamma$ , respectively. If the experimental conditions (i.e. device polarization and ion probe) are maintained constant as well as the ranges of the damaging ions, the NIEL approach can effectively correlate the CCE degradation of an electronic device induced by different radiation sources or energies, as demonstrated in [4][29]. If one or more of these conditions are not fulfilled, the complete expression given by eq. (20) has to be used.

### 3. Experimental and device simulation

#### 3.1. Diode structure

n-type and p-type FZ silicon diodes prepared by the Helsinki Institute of Physics were chosen for characterization of radiation damage induced by MeV energy light ions. Details on the diode structure can be found in [31][32][33].

The n-type samples consist of a  $p^+$  (B implanted, 3.5  $\mu m$  thick) /  $n^-$  ( $\approx 300 \mu m$  thick, FZ grown with resistivity of the order of  $\approx 9 k\Omega \cdot cm$ ) /  $n^+$  (P implanted, 7  $\mu m$  thick) layers. The p-type diodes are  $n^+$  (P implanted, 7  $\mu m$  thick) /  $p^-$  ( $\approx 300 \mu m$  thick, FZ grown with resistivity of the order of  $10 k\Omega \cdot cm$ ) /  $p^+$  (B implanted 3  $\mu m$  thick) junction silicon diodes. All studied samples have a (5 x 5)  $mm^2$  Al-sintered front electrode of 0.42  $\mu m$  thickness, as measured by RBS [34], facing the scanning ion microbeam. The front electrode is surrounded by one main guard ring and 16 thinner guard rings that were floating in all the experiments.

The full depletion voltages ( $V_{fd}$ ) were  $\sim 20$  and 45 V for the n- and p-type diodes, respectively, and the saturated reverse current was about 6 nA for both types. The doping profiles were evaluated by capacitance-voltage characterization assuming an effective area of the electrode of 36  $mm^2$ , which is slightly larger than the geometrical area to take into account the presence of guard rings [31]. The bulk donor and acceptor concentrations of  $3 \cdot 10^{11} cm^{-3}$  and  $5 \cdot 10^{11} cm^{-3}$ , for the n- and p-type diodes respectively, were estimated from capacitance-voltage measurements.



Preliminary characterization of the diodes was performed by IBIC microscopy, adopting the drift-diffusion model [5][35], which provides a direct calculation of the minority carrier diffusion length. J. Garcia et al. [34] obtained the electron diffusion length of the order of 60  $\mu\text{m}$  and the corresponding lifetime of the order of 1  $\mu\text{s}$  for the p-type diodes, which is consistent with the lifetime estimated by microwave probed photoconductivity [36].

### 3.II. Device simulation

The electrostatic and carrier transport parameters were evaluated by solving the Poisson and continuity diode equations [16] by the Finite Element Method [37], assuming the doping profile extracted from capacitance-voltage measurements. A validation of the simulation is shown in Fig. 2a,c, where the experimental capacitance data (markers) are well fitted by the simulated capacitance-voltage curve (continuous line) calculated using the doping profile shown in Fig. 2b,d.

These device simulations were also used to extract the Gunn's weighting field  $\frac{\partial F}{\partial V_s}$  and charge - carrier drift velocities required by the IBIC model, i.e. eq. (20). The Gunn's weighting field was calculated on the basis of the algorithm described in [15]; the Scharfetter and Gummel mobility formula [16] was used to evaluate the electron/hole drift velocity profiles at different bias voltages (Fig. 3).

### 3.III. Diode irradiation

We adopted the established experimental protocol presented in [4] [38], and sketched in Fig. 4 to test the radiation damage induced by 4 and 8 MeV He ions. He ions were focused down to 1  $\mu\text{m}$  spot size and the beam was raster scanned over (100x100  $\mu\text{m}^2$ ) square areas, with fluences up to  $5 \cdot 10^{12}$  ions/ $\text{cm}^2$ . Each fluence was evaluated by direct counting of the charge pulses recorded by a standard charge sensitive electronic chain (e.g. Ortec 142A charge sensitive preamplifiers and Ortec 671 spectroscopy amplifiers) during ion irradiation with typical DIB currents of the order of few fA and dividing the number of recorded pulses by the surface of the particular irradiated area of a device. The uncertainty of the calculated fluence values was less than 1%, mainly due to the dead time of the data acquisition system.

Fig. 5a shows the vacancy profiles of DIBs used in this work (4 MeV and 8 MeV He ions) as calculated by SRIM-2013[8] simulation assuming a displacement energy for silicon of 21 eV [39]. It is

worth noticing that the penetration of 4 and 8 MeV ions in Si is within the depletion region of both diodes.

### 3.IV. Measurement of the CCE degradation

The CCE degradation as a consequence of the ion irradiation produced damage was examined using different low current (several hundred cps) ion beams focused to a micrometre spot size and raster scanned over the diode surface and the previously irradiated regions.

The measurements were carried out in different laboratories (ANSTO [40], SNL [41] , RBI [42]) adopting the commonly used IBIC experimental protocol [4][30] within few days after irradiation, during which the samples were kept at room temperature. The induced charge pulses were acquired during scanning and measured by a conventional charge sensitive electronic chain in different applied bias conditions, using shaping time of the order of 1  $\mu$ s to exclude de-trapping processes.

In order to avoid edge effects, IBIC data were extracted from only central regions (typically 20x20  $\mu$ m<sup>2</sup>) of the irradiated areas. The IBIC spectra corresponding to each fluence value were individually analysed. Since these extracted IBIC spectra were mainly composed of a single peak, they were fitted with a simple Gaussian distribution function. The reported CCE value is the ratio of the Gaussian centroid position and the position of the centroid in a pristine (non-irradiated) sample area. Finally as the result of this off-line analysis of IBIC data, the calculated CCE values were normalized to the CCE of the pristine sample and plotted as function of the DIBs fluence.

The ionization profiles of PIBs used in this paper (2, 8, 12 MeV He ions and 2 and 4.5 MeV protons) are shown in Fig. 5b, as calculated from SRIM-2013 simulations. All generation profiles lie within the depletion region, if the diodes are reverse biased at  $V \geq 10$ V, as demonstrated by comparing Fig. 5 and the insets of Figs 2b and 2d. The exception is the partly damaged p-type diodes reverse biased at  $V_{\text{bias}}=10$  V in the case where the PIB is 4.5 MeV proton, as can be deduced by a comparison of Fig. 5b and the inset of Fig. 2d.

## 4. Results and data analysis

Fig. 6 shows the CCE degradation dependences for p- and n-type diodes irradiated with 8 MeV He ions and probed using different PIBs at different bias voltages applied to the partly-damaged diode under test.

It is apparent that:

- 1  
2  
3  
4 A) For the same PIB, the CCE degradation at a fixed applied bias voltage is more evident for  
5  
6 the lowest reverse bias voltage. This behaviour can be easily interpreted considering that the  
7  
8 effective cross section defined in eq. (25) decreases as a function of the drift velocity which  
9  
10 is function of the applied bias voltage.
- 11 B) The CCE degradation of the p-type diode dependences for 8 MeV He and 2 MeV H PIBs  
12  
13 (Fig. 6a,c) are very similar because both ion probes have the similar normalized ionization  
14  
15 profile  $\gamma(x)$ , defined in eq. (21), as is shown in the inset of Fig.5.
- 16  
17 C) In the cases for which a 4.5 MeV H ion micro-beam was used as the probe, we limit our  
18  
19 analysis only to bias voltages of 20 and 50 V for p-type diodes, in order to consider only  
20  
21 experimental conditions for which our model is valid, in particular the requirement that the  
22  
23 ionization profile is entirely included within the depletion layer to avoid effects due to  
24  
25 diffusion. These CCE degradation dependences on the fluence are weaker than those  
26  
27 discussed in the previous case B). The reason for the lower CCE degradation rate can be  
28  
29 ascribed to the fact that the Bragg peak of the ionization profile occurs deeper than the  
30  
31 vacancy peak and then, the carrier removal is mainly due to minority carrier trapping.

32 In order to implement the model and extract the capture coefficients  $\alpha_{n,p}$ , which characterize the  
33  
34 CCE degradation, we have fitted the experimental data with the expression for CCE, eq. (20), by  
35  
36 scanning the residual (i.e. deviations of the theoretical curve from the experimental points) sum of  
37  
38 squares while varying the parameters  $\alpha_n$  and  $\alpha_p$ . The best fitting parameters are determined by  
39  
40 evaluating the minimum of the resulting residual matrix. Although this rough method can potentially  
41  
42 lead to local minima, it was used because a) it is easy to implement in spite of the complex non-linear  
43  
44 CCE expression in eq. (20) and b) it is possible to combine multiple fitting routines.

45 As an example, Fig. 7a shows the residual matrix relevant to a p-type diode reverse biased at 50 V,  
46  
47 irradiated with 8 MeV He and probed with 2 MeV protons. The residual matrix shows a minima  
48  
49 corresponding to  $\alpha_p=1400 \mu\text{m}^3/\text{s}$ , independently from the  $\alpha_n$  values, since the minima locus lies along a  
50  
51 line parallel to the vertical axis. Actually, since the generation curve is shallower than the damage  
52  
53 profile (see inset in Fig. 5), majority carriers (holes) drift towards the cathode (located at  $x=300 \mu\text{m}$ )  
54  
55 and cross the highly-damaged region located at the vacancy peak, where the recombination probability  
56  
57 is highest. On the other hand, minority carriers (electrons) drift towards the anode ( $x=0$ ). Since their  
58  
59 trajectories develop along the tail of the vacancy profile, their lifetime is very marginally influenced by  
60  
61 the traps induced by radiation damage. This fact is clearly shown in the right side of Fig. 7a, which  
62  
63  
64  
65

represents a plot of the fitted values for two terms of eq. (20), where it is apparent that only hole trapping contributes to the CCE degradation.

On the other hand, if the PIB is more penetrating than DIBs, both majority and minority carriers are being removed by trapping and have an effect on the CCE degradation. The result for such a case is shown by the residual matrix of the p-type diode irradiated with 8 MeV He and probed with 4.5 MeV protons (Fig. 7b).

Finally, combining the two residual matrices, a simultaneous fit of the CCE degradation data corresponding to PIB=2 MeV and 4.5 MeV can be calculated, providing recombination factors of  $\alpha_p=1380 \mu\text{m}^3/\text{s}$  and  $\alpha_n=1860 \mu\text{m}^3/\text{s}$  for holes and electrons, respectively (Fig. 7c).

The solid lines in Fig. 6 are the best fits obtained by the abovementioned procedures considering different PIBs, for p- and n-type diodes reverse biased at 10, 20 and 50 V, respectively.

The final measure of the recombination coefficients is represented in Fig. 8 and summarized in Table I, as evaluated by the combination of all the best fitting parameters.

In the case of a very low damage level, the model given by eq. (28) can be adopted to fit the linear CCE degradation vs. DIB fluence. Moreover, if low penetrating ion probes are used, the term relevant to majority carriers gives the dominant contribution, and the minority carrier term can be neglected.

Fig. 9a shows the linear CCE degradation of an n-type diode irradiated with DIB=8 MeV and 4 MeV He ions at low fluences and probed with PIB=2 MeV He at different bias voltages ( $V=10, 50 \text{ V}$ ). Under these conditions, the model provides the following expression for the CCE linear degradation:

$$(34) \quad \text{CCE}(\Phi) \cong 1 - \alpha_n \cdot \left\{ \Phi \cdot \int_0^d dz \cdot \frac{V(z)}{v_n(z)} \cdot \int_z^d dy \cdot \frac{\partial F(y)}{\partial V_s} \cdot \int_0^z dx \cdot \gamma(x) \right\} = 1 - \alpha_n \cdot \Phi^*$$

It is worth noticing that in this particular case, the nested integrals assume different values as a function of the DIB used, i.e. of the different vacancy profiles  $V(x)$ , and as a function of the applied bias voltage, i.e. of the electron drift velocity and Gunn's weighting field profiles, whereas the generation term  $\gamma(x)$  is the same for all the measurements. Fig. 9c shows similar results for the p-type diode.

The representation of the CCE degradation as function of an "effective fluence"  $\Phi^*$ , defined by the curly bracket in eq. (34), is independent from the experimental conditions (DIB, PIB, diode polarization) used for the CCE measurement of a partly damaged device and allows the visualization of a linear trend, whose slope is the capture coefficient of the majority carriers. This is confirmed by Fig. 9b and Fig. 9d for n- and p-type diodes, respectively, in which it is apparent that the experimental data gather around a unique straight line. The slope of the linear fits provide the measures of the capture

coefficient  $\alpha_p=(1420\pm150) \mu\text{m}^3/\text{s}$  and  $\alpha_n=(2500\pm400) \mu\text{m}^3/\text{s}$  for p- and n-type diodes, which are compatible with the values measured on similar diodes with more penetrating PIBs (Fig. 8 and Table I). Finally, in order to test the stability and reliability of the measurements, the diodes were annealed at 80°C for 2 hours according to the American Society for Testing and Materials (ASTM) standard [43]. No remarkable deviation in the CCE degradation was observed, reproducing the measurements under the same experimental conditions.

## 5. Discussion and conclusions

This work shows the results of a research project coordinated by IAEA involving different institutes, which is aimed to define an experimental protocol and elaborate an interpretative model of the CCE degradation of semiconductor devices irradiated with MeV ions. The experimental procedure, based on the previous work [4] was applied to study the radiation hardness of silicon n- and p-type diodes using 8 MeV and 4 MeV He ion microbeams to selectively irradiate small (with respect to the device size) areas (typically  $(100\times100) \mu\text{m}^2$ ) of the devices at different fluences. The main advantage of this experimental approach is that the reduced sizes of these irradiated regions, allows the same diode to be irradiated with different DIBs at different fluences and the CCE degradation to be measured with different PIBs.

The CCE vs. fluence of selectively irradiated devices were measured by the IBIC technique using low current H and He MeV ion beams with different energies and applying different bias voltages. The main advantages of this experimental methodology lie in the operational simplicity, since the radiation hardness test can be performed on a single device using damaging ions with different mass, energies and at different fluences. Moreover, because of the smallness of the damaged region with respect to the active volume of the device, the increase of dark current and of the detection noise is negligible.

The results summarized in Fig. 6 and Fig. 9 show different CCE degradation behaviours depending both on the PIB energies and diode polarization conditions.

In order to provide a comprehensive interpretation of all these data, we have developed a general model, which integrates the Shockley-Read-Hall recombination model (10) into the Shockley-Ramo-Gunn theory (6). The model provides a set of differential equations, whose solution is the CCE vs. the ion irradiation fluence dependence. The limits of validity of such an approach are defined in the section 2.

The experiments described in this paper, have been designed to fulfil these requirements. In particular, we have used weakly ionizing PIBs, whose ionizing tracks lie within the regions with

localized strong electric fields, in order to minimize plasma effects [44]. Although we have neither experimental evidence, nor theoretical arguments, that clearly justify the assumption of negligible plasma and/or high charge injection effects.

Nevertheless, this assumption can be reasonably motivated by noting that:

- The ionization occurs within the depletion region, so no funneling effects [5] are expected
- The CCE degradation curve, for each PIB, is normalized to the pristine case; therefore, plasma effects should perturb the induced charge collection mechanism of the same fraction, independently from the (low) level of damage. Therefore, the CCE degradation curves measured using a single ion specie is self-consistent, i.e. unaffected from plasma effects.
- Inconsistences may arise from a comparison of CCE degradation curves measured with different PIBs. Actually, the maxima of the linear energy transfer range from 65 keV/ $\mu\text{m}$  for 4.5 MeV H to 330 keV/ $\mu\text{m}$  for 8 MeV He. However, possible differences on plasma effects can be compensated by the different localization of the Bragg peaks, since the highest electron/hole densities occur with the highest electric field, which can rapidly erode the plasma column.

The model considers the generation of recombination centres as the only effect induced by atomic displacements resulting from the interaction of the incoming ion and the atomic lattice. The resulting carrier lifetimes are connected to the ion fluence through eq. (10), which implies a trap distribution, which is proportional to the distribution of vacancies created initially by the radiation. Moreover, it is assumed that transport properties (i.e. carrier mobilities) and the effective doping concentration (and then the electric field) are not affected by ion irradiation.

Regarding this latter point, some publications have provided evidence for the influence of MeV ion irradiation on the effective doping of the highly resistive FZ silicon diodes under test [31][42]. However, it is worth emphasising that those experiments were performed with MeV proton irradiation, which effectively perturb the pristine doping distribution of n-type materials through the generation of acceptor-like defects and hydrogen related excess donors [45]. Despite having used alpha particles and not protons as DIBs, in order to check this point, we have irradiated the whole electrode of both p- and n- diodes with 8 MeV He ions at a fluence of  $2 \times 10^{11} \text{ cm}^{-2}$  with the aim of comparing the resulting doping profile from capacitance-voltage characteristics measured on pristine and irradiated diodes. The drastic increase of leakage current for both the n-type and p-type diodes of more than two orders of magnitudes prevented a reliable comparison of the effects of irradiation on the effective doping profiles. However, to corroborate the validity of our results, it is worth mentioning that the CCE

1  
2  
3  
4 degradations carried out in different experimental conditions and at different damaging ion fluences  
5 (summarized in Fig. 6 and Fig. 9) provide compatible measures of the capture coefficients, which were  
6 confirmed also after annealing the samples as prescribed by [43].  
7  
8

9  
10 In summary, the above mentioned requirements define the condition of “low level of damage” we  
11 adopted in this work. The model we have developed can be effectively used only in this regime. The  
12 case of high level of damage relevant to majority carrier compensation due to carrier removal process,  
13 can in principle be treated on a similar basis, by means of a dynamical upgrading of the device  
14 electrostatics, which is progressively perturbed by the generation of charged defects as function of the  
15 ion fluence. However, this extension of the model is beyond the scope of this work and will not be  
16 further discussed.  
17  
18

19  
20 In the case of devices with depletion regions extending deeper than the probing and damaging ion  
21 range, the set of equations (6) limited to only one dimension (14), can be solved and an analytical  
22 expression of the CCE can be calculated as function of the damaging ion fluence, DIBs vacancy and  
23 PIB generation profiles and of the electrostatic and transport features of the device (20). This solution  
24 models the charge induced at the sensing electrode of individual charge carriers (electrons and holes),  
25 which drift toward the electrode within a variable velocity field and undergo recombination, which is  
26 particularly effective at the stopping range of DIBs, where is located at the Frenkel pairs density peak.  
27 The opposite drift directions of electrons and holes, allow the contribution of the two (minority and  
28 majority) carriers to be discriminated, depending on the generation profile induced by ionization of the  
29 PIBs.  
30  
31

32  
33 The resulting formulation is quite general and includes both the generalized Hecht’s formula and the  
34 NIEL displacement damage formulas as special cases (see sections 2.II and 2.III) regarding low level  
35 of damage and constant electric fields.  
36  
37

38  
39 The methodology adopted to fit the experimental data with the theoretical curves proved to be  
40 effective to evaluate the two fitting parameters, namely the capture coefficients  $\alpha_{n,p}$  (23), which provide  
41 the key parameters for the characterization of the effects of radiation damage in semiconductors.  
42 Actually, they depend on 1) the capture cross sections  $\sigma_{n,p}$ , which identify the nature of the  
43 recombination centres and 2) the factor  $k_{n,p}$ , which is the proportional factor connecting the active  
44 recombination centres with the concentration of Frenkel pairs introduced as primary point defects.  
45 Since primary defects are mostly created by cascading-displacement processes, the  $k_{n,p}$  factors are  
46 assumed independent on the type of the incoming particles [2]. Assuming  $v_n^{\text{th}} = 2.05 \cdot 10^7 \text{ cm/s}$   
47  
48  
49  
50  
51  
52  
53  
54  
55  
56  
57  
58  
59  
60  
61  
62  
63  
64  
65

and  $v_p^{th} = 1.69 \cdot 10^7$  cm/s [46], the  $k_{n,p} \cdot \sigma_{n,p}$  products, calculated from the fitting of the experimental data, are summarized in Table I.

The capture coefficient of majority carriers for the p-type diode is smaller than the capture coefficient for the n-type diode as calculated from these data. This is clearly evidenced by the CCE degradation as a function of the effective fluence  $\Phi^*$  measured with the short penetration PIB (2 MeV He ions) which is shown in Fig. 9b, d. This result seems to contradict the CCE degradation plotted as function of the ion fluence in Fig. 9a,c or, by comparison of the data related to the PIB=2 MeV H shown in Fig. 6a,b, where the CCE degradation is steeper for p-type than for n-type diode. The reason of this apparent contradiction stems from the fact that the CCE degradation depends on the effective capture cross sections (eq. (25) ), which is inversely proportional to the carrier velocity. Therefore, by virtue of the “(1/v) law” [26], electron recombination is less probable than hole recombination, because the drift velocity is higher for electrons than for holes. The main conclusions that can be drawn from these findings is that the method has the potential to estimate the intrinsic radiation hardness of the material, and not of the specific device, whose performances depend not only on the irradiation type, but also on the diode polarization conditions and on the probing ion species.

Finally, the analysis can be further enriched by extracting, from the  $k \cdot \sigma$  measured values, more information on the k-factor, i.e. on the efficiency of Frenkel pairs to produce stable recombination centres, if the intrinsic capture cross sections  $\sigma_{n,p}$  are available. These values can be obtained by Deep Level Transient Spectroscopy [47] or similar techniques based on scanning ion beams [48] [49]. DLTS studies performed on an n-type diode irradiated by 8 MeV He ions at a fluence of  $10^{10}$  cm<sup>-2</sup> show a typical Si displacement damaged spectrum with dominant di-vacancy peaks (see for example [50]). If the relevant capture cross section values for electrons ( $\sigma_n = 5 \cdot 10^{-15}$  cm<sup>-2</sup>) and holes ( $\sigma_p = 5 \cdot 10^{-14}$  cm<sup>-2</sup>) [51], are assumed, the k-terms are  $k_n = 2.4 \cdot 10^{-2}$  and  $k_p = 2.4 \cdot 10^{-4}$ , i.e. about 40 and 4,000 radiation induced defects are required to form 1 stable electron and hole recombination centre, respectively.

However, this result has to be interpreted carefully, because it is strictly connected with the absolute vacancy profiles  $V(x)$  used in this work and evaluated through the SRIM simulation. This widely used code is based on the Binary Collision Approximation (BCA) and uses the Displacement Energy Threshold ( $E_d$ ) parameter as the energy needed to displace an atom from the lattice to create a stable Frenkel pair [52]. However, SRIM considers the target as amorphous, whereas the density functional theory (DFT) molecular dynamics (MD) simulations [53] have demonstrated that  $E_d$  varies in the range of 12-36 eV with preferred direction of recoil. As an example aimed to demonstrate the impact of this ambiguity on the quantitative results of our work, SRIM gives the number of vacancies created by 8



MeV He irradiation of Si as 435, 256, and 145 for the values of 13, 21, and 36 eV for  $E_d$ , respectively. Since the relative vacancy profile is maintained, the adoption of the former and latter values of  $E_d$  provide a scale factor of 1.7 and 0.56, respectively, for the values of the capture coefficient  $\alpha_{n,p}$  with respect to the values listed in Table I and calculated adopting  $E_d = 21$  eV.

To take into account the crystal structure of the target material, the MARLOWE crystal BCA code [19] can be used. This code uses the binding energy parameter and keeps track of the positions of all vacancies and interstitials produced within one cascade. After all cascade atoms have come to rest, the cascade atoms and lattice sites involved are arranged in Frenkel pairs and sorted into classes. In order to precisely determine the distance among vacancy/interstitial pairs, which yield permanent displacements and stable defects, the concept of recombination radius has been recently introduced and estimated by a direct comparison with MD calculations [54].

Moreover, it is worth emphasizing that neither SRIM nor MARLOWE take into account the diffusion of Frenkel pairs produced along the tracks of the recoil primary atoms to form stable defects at room temperature. Assuming that the capture time of a vacancy on an impurity is about 1 s in normal silicon at room temperature [55], since the irradiated sample was kept at room temperature for few days between the ion irradiation and the IBIC measurement of CCE degradation, we cannot neglect the fact that defect migration and the capture of vacancies by impurities and self-interstitials can remarkably influence the actual absolute defect distribution from the evaluation of a BCA code.

From these considerations, the amount of damage calculated by SRIM must be considered as the maximum that can be observed from the kinetic effects of the ion on the target atoms. As a consequence, the vacancy profile  $V(x)$  used for our data analysis (eq.(20)), must be considered as overestimated (i.e. the  $k \cdot \sigma$  products shown in Table I are underestimated).

However, these drawbacks do not invalidate the methodology described in this work. If we assume that SRIM provides realistic but un-normalized vacancy and ionization profiles, the capture coefficients extracted from the fitting procedure can be considered reference values, which can be used to compare the radiation hardness of different semiconductor devices and envisage the corresponding CCE degradation for any ion irradiation and polarization condition. An exhaustive connection of these parameters with the nature and the number of stable radiation induced defects require the use of more elaborate computational tools and experimental techniques.

It is beyond the scope of this paper to explore this vast field. Here we have limited ourselves to present the theoretical and experimental approach for the characterization of the displacement damage effects on the electronic performance of semiconductor devices. This work can be considered as an

extension of the NIEL approach, which can be inferred from our model in the case of constant damage profile.

## 6. Acknowledgements

This work has been carried out within the IAEA Coordinated Research Project No. F11016 “Utilization of Ion Accelerators for Studying and Modelling Ion Induced Radiation Defects in Semiconductors and Insulators” and has been supported in part by Croatian Science Foundation under the project MIOBICC (8127).

## 7. References

- [1] IAEA CRP n. F11016, <http://cra.iaea.org/cra/explore-crps/all-active-by-programme.html>
- [2] C. Leroy, P.G. Rancoita, Particle interaction and displacement damage in silicon devices operated in radiation environments, *Rep. Prog. Phys.* 70 (2007), 493-625.
- [3] J.G. Laven, H.-J. Schulze, V. Häublein, F.-J. Niedernostheide, H. Schulze, H. Ryssel, et al., Deep Doping Profiles in Silicon Created by MeV Hydrogen Implantation: Influence of Implantation Parameters, 257 (2011) 257–260. doi:10.1063/1.3548365.
- [4] Z. Pastuović, E. Vittone, I. Capan, M. Jakšić, Probability of divacancy trap production in silicon diodes exposed to focused ion beam irradiation, *Appl. Phys. Lett.* 98 (2011) 2–4. doi:10.1063/1.3559000.
- [5] M.B.H. Breese, E. Vittone, G. Vizkelethy, P.J. Sellin, A review of ion beam induced charge microscopy, *Nucl. Instruments Methods Phys. Res. Sect. B Beam Interact. with Mater. Atoms.* 264 (2007) 345–360. doi:10.1016/j.nimb.2007.09.031.
- [6] E. Vittone, “Semiconductor Characterization by Scanning Ion Beam Induced Charge (IBIC) Microscopy”, spotlight paper of *ISRN Materials Science*, vol. 2013, 637608 (2013), <http://downloads.hindawi.com/isrn/ms/2013/637608.pdf>.
- [7] W. Shockley, W.T. Read, Statistics of the Recombination of Holes and Electrons, *Phys. Rev.* 87 (1952) 835–842. doi:dx.doi.org/10.1103/PhysRev.87.835.
- [8] J.F. Ziegler, J.P. Biersack, M.D. Ziegler, “SRIM – The Stopping and Range of Ions in Matter”, Ion Implantation Press, 2008. <http://www.lulu.com/content/1524197>.
- [9] E. Vittone, Z. Pastuovic, P. Olivero, C. Manfredotti, M. Jaksic, a. Lo Giudice, et al., Semiconductor characterization by scanning ion beam induced charge (IBIC) microscopy, *Nucl. Instruments Methods Phys. Res. Sect. B Beam Interact. with Mater. Atoms.* 266 (2008) 1312–1318. doi:10.1016/j.nimb.2007.12.083.

- [10] G. Vizkelethy, Simulation of ion beam induced current in radiation detectors and microelectronic devices, Nucl. Instruments Methods Phys. Res. Sect. B Beam Interact. with Mater. Atoms. 269 (2011) 2330–2335. doi:10.1016/j.nimb.2011.02.045.
- [11] T.H. Prettyman, Theoretical framework for mapping pulse shapes in semiconductor radiation detectors, Nucl. Instruments Methods Phys. Res. Sect. A Accel. Spectrometers, Detect. Assoc. Equip. 428 (1999) 72–80. doi:10.1016/S0168-9002(98)01582-4.
- [12] T.H. Prettyman, Method for mapping charge pulses in semiconductor radiation detectors, Nucl. Instruments Methods Phys. Res. Sect. A Accel. Spectrometers, Detect. Assoc. Equip. 422 (1999) 232–237. doi:10.1016/S0168-9002(98)01100-0. J.B.Gunn, Solid-State Electronics, 7 (1964), 739-742.
- [13] J.B. Gunn, A general expression for electrostatic induction and its application to semiconductor devices, Solid State Electronics 7 (10) (1964) 739-742.
- [14] E. Vittone, Theory of ion beam induced charge measurement in semiconductor devices based on the Gunn's theorem, Nucl. Instruments Methods Phys. Res. Sect. B Beam Interact. with Mater. Atoms. 219-220 (2004) 1043–1050. doi:10.1016/j.nimb.2004.01.210.
- [15] L. Grassi, J. Forneris, D. Torresi, L. Acosta, a. Di Pietro, P. Figuera, et al., Study of the inter-strip gap effects on the response of Double Sided Silicon Strip Detectors using proton micro-beams, Nucl. Instruments Methods Phys. Res. Sect. A Accel. Spectrometers, Detect. Assoc. Equip. 767 (2014) 99–111. doi:10.1016/j.nima.2014.08.009..
- [16] S. Selberherr. *Analysis and Simulation of Semiconductor Devices*, Springer-Verlag, Wien-New York, ISBN 978-3-7091-8754-8, 1984.
- [17] C. Manfredotti, F. Fizzotti, a. Lo Giudice, M. Jaksic, Z. Pastuovic, C. Paolini, E. Vittone et al., Time-resolved ion beam-induced charge collection measurement of minority carrier lifetime in semiconductor power devices by using Gunn's theorem, Mater. Sci. Eng. B Solid-State Mater. Adv. Technol. 102 (2003) 193–197. doi:10.1016/S0921-5107(02)00656-6.
- [18] Chih-Tang Sah, *Fundamentals of Solid-State Electronics*, World Scientific, Singapore 1991.
- [19] M.T. Robinson, I.M. Torrens, Computer simulation of atomic-displacement cascades in solids in the binary-collision approximation, Phys. Rev. B. 9 (1974) 5008–5024.

- [20] Gerhard Lutz, *Semiconductor Radiation Detectors: Device Physics*, Springer Science & Business Media, (1999).
- [21] M. Martini, T.W.Raudorf, W.R. Stott, J.C. Waddington, "Comparitive Ionization Energies for Protons, Deuterons and Alpha Particles in High Purity Germanium and Si(Li) Nuclear Radiation Detectors," IEEE Transactions on Nuclear Science, 22, (1) (1975), 145-148. doi: 10.1109/TNS.1975.4327632
- [22] W. Shockley, Currents to conductors induced by a moving point charge, J. Appl. Phys. 9, (1938) 635–636
- [23] S. Ramo, Currents induced by electron motion. Proc. IRE. 27, (1939), 584–585
- [24] V. Radeka, Low-Noise Techniques, Annu. Rev. Nucl. Part. Sci. (1988) 217–277.
- [25] E. Vittone, F. Fizzotti, a. Lo Giudice, C. Paolini, C. Manfredotti, Theory of ion beam induced charge collection in detectors based on the extended Shockley-Ramo theorem, Nucl. Instruments Methods Phys. Res. Sect. B Beam Interact. with Mater. Atoms. 161 (2000) 446–451. doi:10.1016/S0168-583X(99)01000-9.
- [26] E. Amaldi, O. D’Agostino, E. Fermi, B. Pontecorvo, F. Rasetti, E. Segrè, Artificial Radioactivity produced by Neutron Bombardment - II, Proc. R. Soc. Lond. A. Math. Phys. Sci. A149 (1935) 522–558.
- [27] S.R. Messenger, E. a. Burke, G.P. Summers, M. a. Xapsos, R.J. Walters, E.M. Jackson, et al., Nonionizing Energy Loss (NIEL) for Heavy Ions, IEEE Trans. Nucl. Sci. 46 (1999) 1595–1602.
- [28] S.R. Messenger, E. Burke, R.J. Walters, J.H. Warner, G.P. Summers, Using SRIM to calculate the relative damage coefficients for solar cells, Prog. Photovoltaics Res. Appl. 13 (2005) 115–123. doi:10.1002/pip.608.
- [29] G.P. Summers, E. a. Burke, M. a. Xapsos, Displacement Damage Analogs to Ionizing Radiation Effects, Radiat. Meas. 24 (1995) 1–8.
- [30] Z. Pastuović, M. Jaksic, E. Vittone, Ion Beam Induced Charge analysis of radiation damage in silicon, Micro- Nanotechnol. Sensors, Syst. Appl. V, Proc. SPIE. 8725 (2013) 87251
- [31] A.S. Väyrynen, J. Räisänen, I. Kassamakov, E. Tuominen, Breakdown of silicon particle detectors under proton irradiation, J. Appl. Phys. 106 (2009) 104914. doi:10.1063/1.3262611.

- [32] S. Väyrynen, J. Räisänen, Effect of proton energy on damage generation in irradiated silicon, *J. Appl. Phys.* 107 (2010) 1–5. doi:10.1063/1.3371714.
- [33] S. Väyrynen, J. Räisänen, P. Tikkanen, I. Kassamakov, E. Tuominen, Effects of activation by proton irradiation on silicon particle detector electric characteristics, *J. Appl. Phys.* 106 (2009) 024908. doi:10.1063/1.3168436.
- [34] J. Garcia Lopez, M.C. Jimenez-Ramos, Charge collection efficiency degradation on Si diodes irradiated with high energy protons, *Nucl. Instruments Methods Phys. Res. Sect. B Beam Interact. with Mater. Atoms.* 332 (2014) 220–223. doi:10.1016/j.nimb.2014.02.065.
- [35] M.B.H. Breese, A theory of ion beam induced charge collection, *J. Appl. Phys.* 74 (1993) 3789–3799.
- [36] E. Gaubas, T. Čeponis, a. Uleckas, J. Vaitkus, J. Raisanen, Recombination characteristics in 2–3MeV protons irradiated FZ Si, *Nucl. Instruments Methods Phys. Res. Sect. A Accel. Spectrometers, Detect. Assoc. Equip.* 612 (2010) 559–562. doi:10.1016/j.nima.2009.08.013.
- [37] COMSOL: Multiphysics Modeling and Simulation, ver. 3.5. [www.comsol.com](http://www.comsol.com).
- [38] A. Simon, G. Kalinka, Investigation of charge collection in a silicon PIN photodiode, *Nucl. Instruments Methods Phys. Res. Sect. B Beam Interact. with Mater. Atoms.* 231 (2005) 507–512. doi:10.1016/j.nimb.2005.01.108.
- [39] J.W. Corbett, G.D. Watkins, Production of divacancies and vacancies by electron irradiation of silicon, *Phys. Rev.* 138 (1965). doi:10.1103/PhysRev.138.A555.
- [40] Ž. Pastuović, I. Capan, R. Siegele, R. Jačimović, J. Forneris, D.D. Cohen, et al., Generation of vacancy cluster-related defects during single MeV silicon ion implantation of silicon, *Nucl. Instruments Methods Phys. Res. Sect. B Beam Interact. with Mater. Atoms.* 332 (2014) 298–302. doi:10.1016/j.nimb.2014.02.082.
- [41] G. Vizkelethy, R.M. Fleming, E. Bielejec, Investigation of ion beam induced radiation damage in Si PN diodes, *Nucl. Instruments Methods Phys. Res. Sect. B Beam Interact. with Mater. Atoms.* 306 (2013) 176–180. doi:10.1016/j.nimb.2012.12.036.
- [42] N. Barbero, J. Forneris, V. Grilj, M. Jakšić, J. Räisänen, A. Simon, et al., Degradation of the charge collection efficiency of an n-type Fz silicon diode subjected to MeV proton irradiation, *Nucl. Instruments Methods Phys. Res. Sect. B Beam Interact. with Mater. Atoms.* 348 (2014) 260–264. doi:10.1016/j.nimb.2014.11.019.

- [43] ASTM, E1854-07 Standard Practice for Ensuring Test Consistency in Neutron-Induced Displacement Damage of Electronic Parts, ASTM Standards, ASTM International (<http://www.astm.org>), 2007.
- [44] P. A. Tove, W. Seibt (1967). "Plasma Effects in Semiconductor Detectors." *Nuclear Instruments & Methods* 51 (1967) (2): 261-269
- [45] J.G. Laven, R. Job, H.-J. Schulze, F.-J. Niedernostheide, W. Schustereder, L. Frey, Activation and Dissociation of Proton-Induced Donor Profiles in Silicon, *ECS J. Solid State Sci. Technol.* 2 (2013) P389–P394. doi:10.1149/2.028309jss..
- [46] M. A. Green, Intrinsic concentration, effective densities of states, and effective mass in silicon, *J. Appl. Phys.* 67, 2944 (1990).
- [47] D.V. Lang, Deep-level transient spectroscopy: a new method to characterize traps in semiconductors *J. Appl. Phys.*, 45 (1974), pp. 3023–3032.
- [48] J.S. Laird, R.A. Bardos. C. Jagadish, D.N. Jamieson, G.J.F. Legge, Scanning ion deep level transient spectroscopy, *Nucl. Instruments Methods Phys. Res. Sect. B Beam Interact. with Mater. Atoms.* 158 (1999) 464–469, doi: 10.1016/S0168-583X(99)00329-8.
- [49] W. Kada, Y. Kambayashi, N. Iwamoto, S. Onoda, T. Makino, M. Koka, T. Kamiya, N. Hoshino, H. Tsuchida, K. Kojima, O. Hanaizumi, T. Ohshima, Development of diagnostic method for deep levels in semiconductors using charge induced by heavy ion microbeams, *Nucl. Instruments Methods Phys. Res. Sect. B Beam Interact. with Mater. Atoms.* 348 (2015) 240–245, doi:10.1016/j.nimb.2014.12.054.
- [50] R.M. Fleming, C.H. Seager, D. V. Lang, E. Bielejec, J.M. Campbell, Defect-driven gain bistability in neutron damaged, silicon bipolar transistors, *Appl. Phys. Lett.* 90 (2007). doi:10.1063/1.2731516.
- [51] L. Vines, E. V. Monakhov, J. Jensen, a. Y. Kuznetsov, B.G. Svensson, Effect of spatial defect distribution on the electrical behavior of prominent vacancy point defects in swift-ion implanted Si, *Phys. Rev. B - Condens. Matter Mater. Phys.* 79 (2009) 1–9. doi:10.1103/PhysRevB.79.075206.
- [52] G.H. Kinchin, R.S. Pease, The displacement of atoms in solids by radiation, *Rep. Prog. Phys.* 18 (1955) 1. doi:10.1007/BF02744350.
- [53] E. Holmström, a. Kuronen, K. Nordlund, Threshold defect production in silicon determined by density functional theory molecular dynamics simulations, *Phys. Rev. B - Condens. Matter Mater. Phys.* 78 (2008) 1–6. doi:10.1103/PhysRevB.78.045202.

- 1  
2  
3  
4 [54] G. Vizkelethy, S.M.Foiles, Determination of recombination radius in Si for binary  
5 collision approximation codes, to be published in Nucl. Instruments Methods Phys. Res.  
6 Sect. B; DOI: 10.1016/j.nimb.2015.08.088  
7  
8  
9  
10 [55] M. Huhtinen, Simulation of non-ionising energy loss and defect formation in silicon,  
11 Nucl. Instruments Methods Phys. Res. Sect. A Accel. Spectrometers, Detect. Assoc.  
12 Equip. 491 (2002) 194–215. doi:10.1016/S0168-9002(02)01227-5.  
13  
14  
15  
16  
17  
18  
19  
20  
21  
22  
23  
24  
25  
26  
27  
28  
29  
30  
31  
32  
33  
34  
35  
36  
37  
38  
39  
40  
41  
42  
43  
44  
45  
46  
47  
48  
49  
50  
51  
52  
53  
54  
55  
56  
57  
58  
59  
60  
61  
62  
63  
64  
65

## 8. Figure Captions

- Fig. 1 a) Schematics of the one-dimensional geometry; b) Schematics of a p<sup>+</sup>/n/n<sup>+</sup> junction diode, irradiated with DIBs, which induce a vacancy profile  $V(x)$  (graph i) peaked more deeply than the generation profile  $\gamma(x)$  (graph ii).
- Fig. 2 Capacitance-Voltage characteristics (a,c) and doping profiles (b,d) of n- and p-type diodes; the insets show the relevant behaviours of the depletion layer width as function of the applied bias voltage (axes exchanged). Markers: experimental data; error bars are smaller than the marker size; Line: Finite Element Method calculations
- Fig. 3 (a,c) Gunn weighting field and (b,d) carrier velocity profiles of n-type (top) and p-type (bottom) diodes..
- Fig. 4 Schematics of the experimental protocol adopted in this work: the diode (a) was first raster scanned with DIBs in order to individuate a region with uniform CCE (b). Nine regions were selected and irradiated with DIBs at different fluences ( $\Phi_1 \dots \Phi_9$ ) (c). PIB ions were then used to probe the CCE degradation in the damaged regions (d) and pulse height spectra were then extracted at different bias voltages from their central zone (e). Finally, the centroids of the spectra were plotted as function of the DIBs fluence (f)..
- Fig. 5 (a) vacancy profiles for the DIBs and (b) ionization profiles for PIBs from SRIM-2013 simulations. Inset: zoom for PIBs 8MeV He from Fig. 5b) (right axis) and 2 MeV H and DIB= 8 MeV He from Fig 5a) (linear scale, left axis).
- Fig. 6 CCE degradation of p-type (left column) and n-type (right column) diodes measured at different bias voltages using different PIBs: a,b) 2 MeV H, c) 8 MeV He, d) 12 MeV He, e,f) 4.5 MeV H. Markers: experimental data; line: fitting curves calculated by means of eq. (20), assuming as fitting parameters the capture coefficients  $\alpha_n$  and  $\alpha_p$ .
- Fig. 7 (left) Normalized residual matrix contour plots relevant to (a) 2 MeV H, (b) 4.5 MeV H ion probes. The contour plot (c) is relevant to the combination of the two previous matrices. (right) Corresponding experimental data and fitting curves (solid lines). Dashed and dotted lines are the electron and hole contributions, respectively.
- Fig. 8 Final measurement of the recombination coefficients; n-type diode:  $\alpha_p=(210\pm160)\mu\text{m}^3/\text{s}$ ;  $\alpha_n=(2500\pm300)\mu\text{m}^3/\text{s}$ ; p-type diode:  $\alpha_n=(2200\pm300)\mu\text{m}^3/\text{s}$ ;  $\alpha_p=(1310\pm90)\mu\text{m}^3/\text{s}$ ; Open marks: dispersion of the combination of the fitting parameters.
- Fig. 9 CCE degradation (DIB=4 MeV and 8 MeV He; PIB=2 MeV He) as function of fluence (a,c) and of the effective fluence (b,d) for n-type and p-type diodes, respectively.



## 9. Table Caption

Table I. capture coefficients and  $k \cdot \sigma$  products resulting from the fitting procedure

	$\alpha_n$ ( $10^{-12}$ cm <sup>3</sup> /s)	$k_n \cdot \sigma_n$ ( $10^{-16}$ cm <sup>2</sup> )	$\alpha_p$ ( $10^{-12}$ cm <sup>3</sup> /s)	$k_p \cdot \sigma_p$ ( $10^{-16}$ cm <sup>2</sup> )
n-type	2500±300	1.21±0.15	210±160	0,12±0.09
p-type	2200±300	1.00±0.15	1310±90	0.77±0.05
Table I: capture coefficients and $k \cdot \sigma$ products resulting from the fitting procedure				

Figure

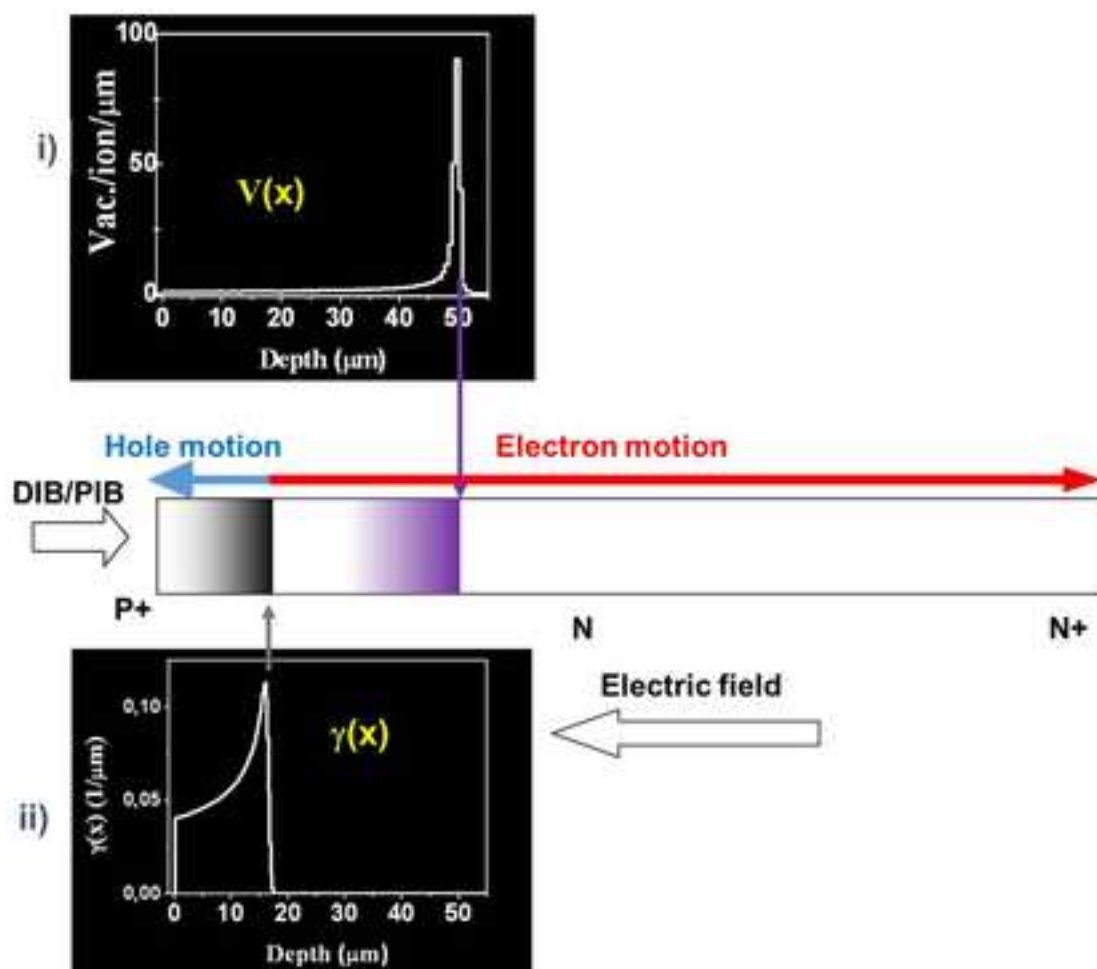
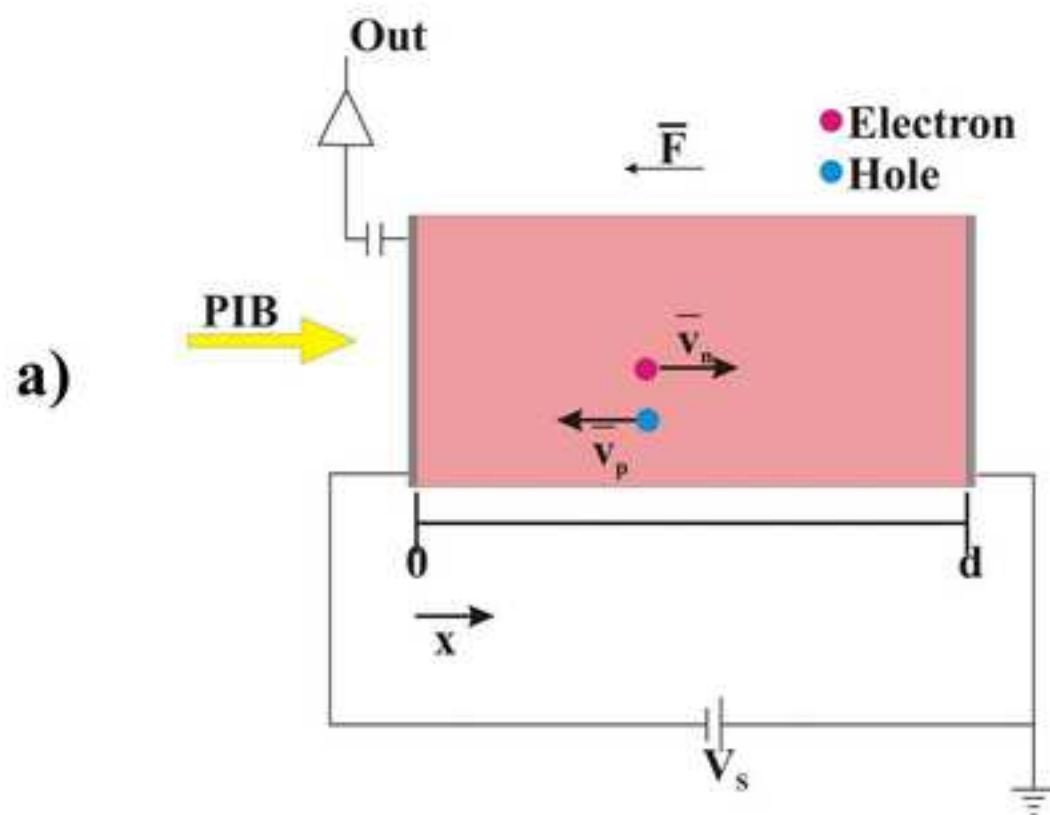


Figure2

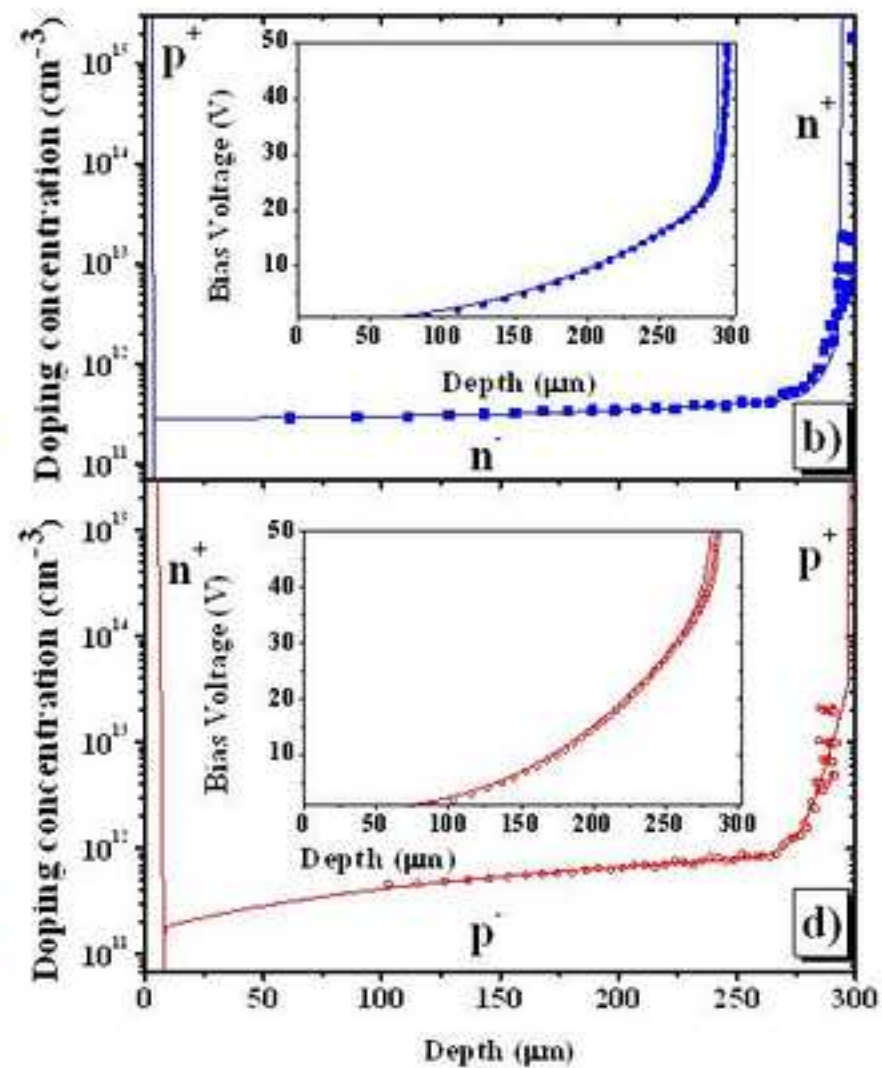
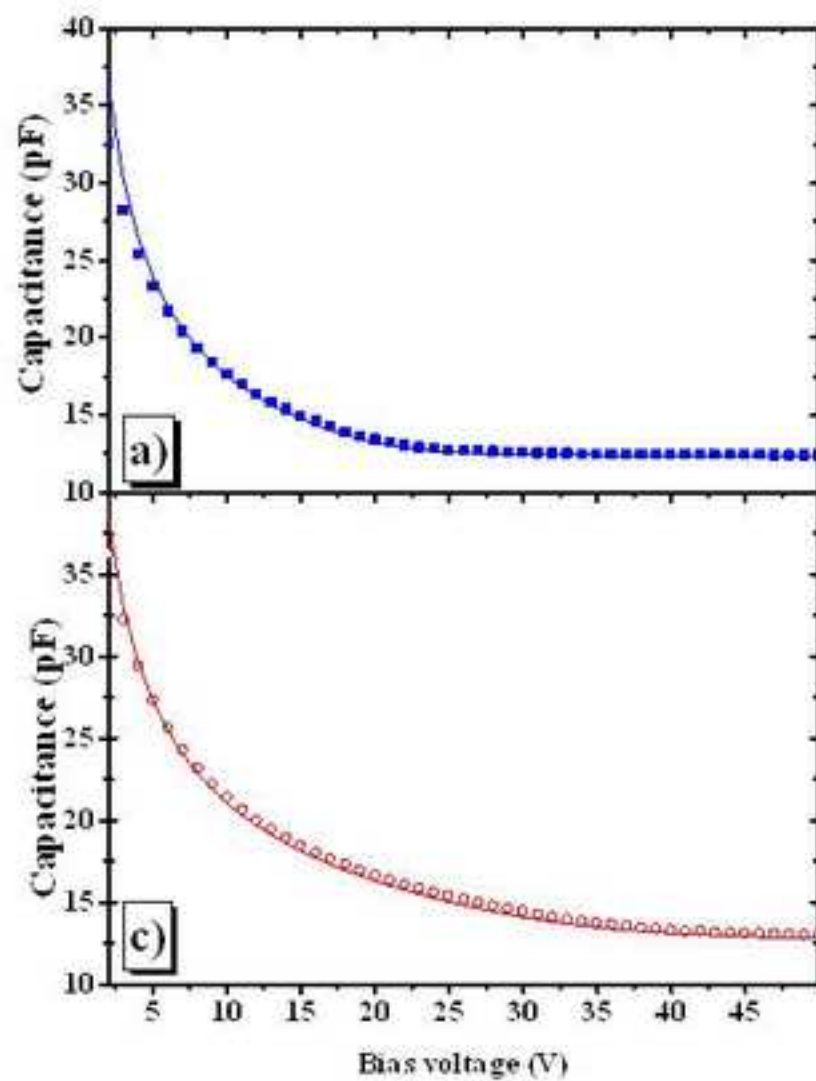


Figure3

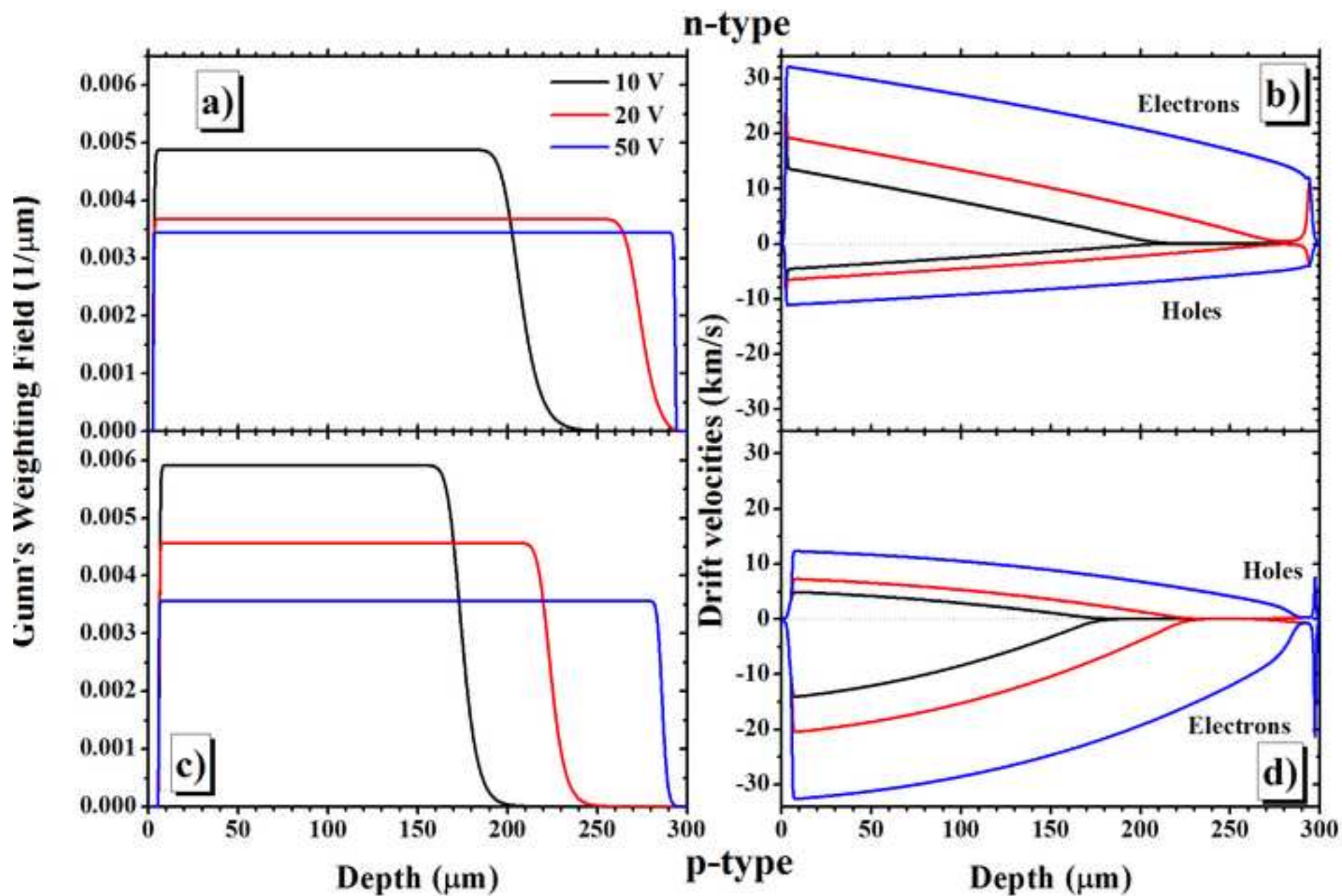


Figure4

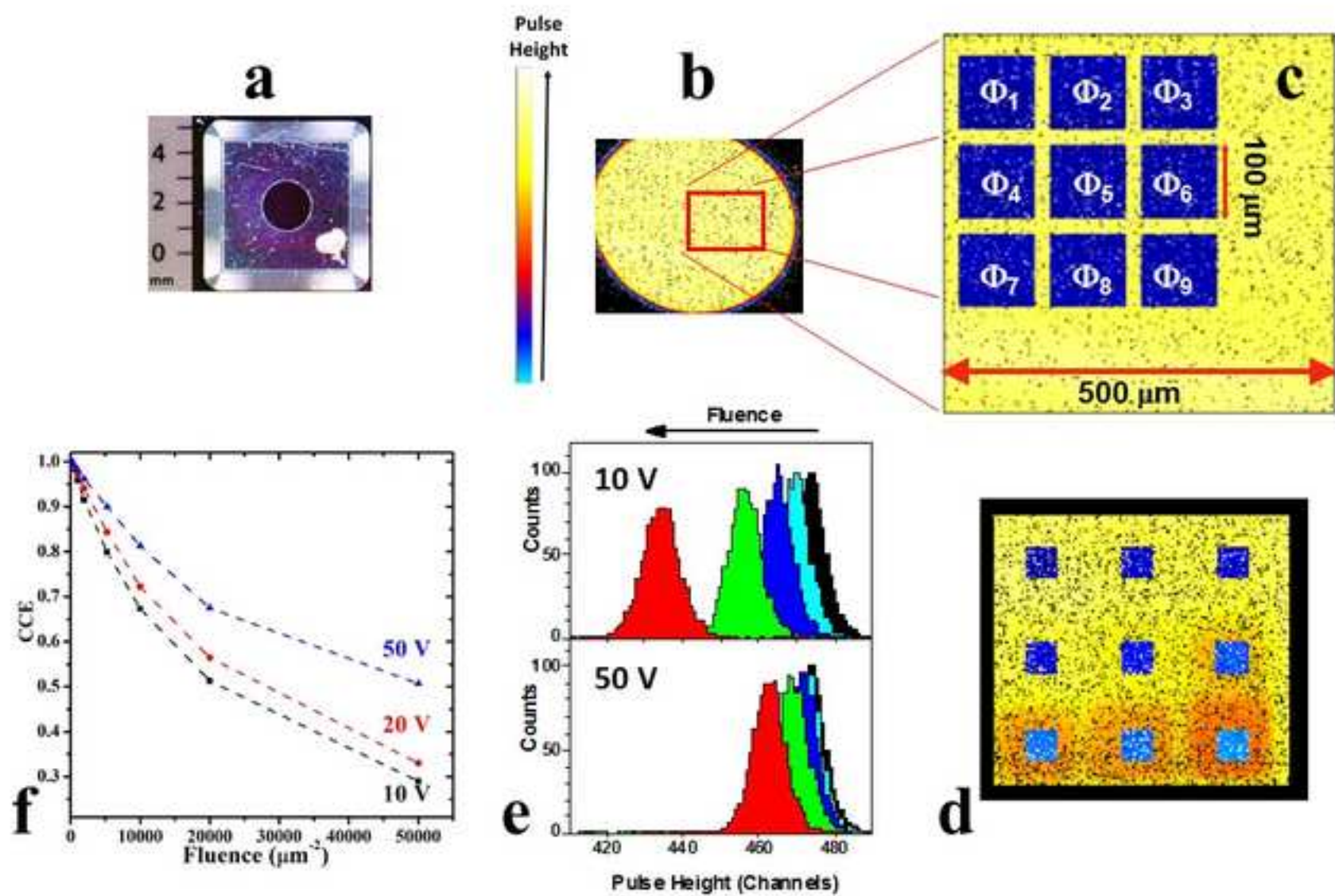




Figure5

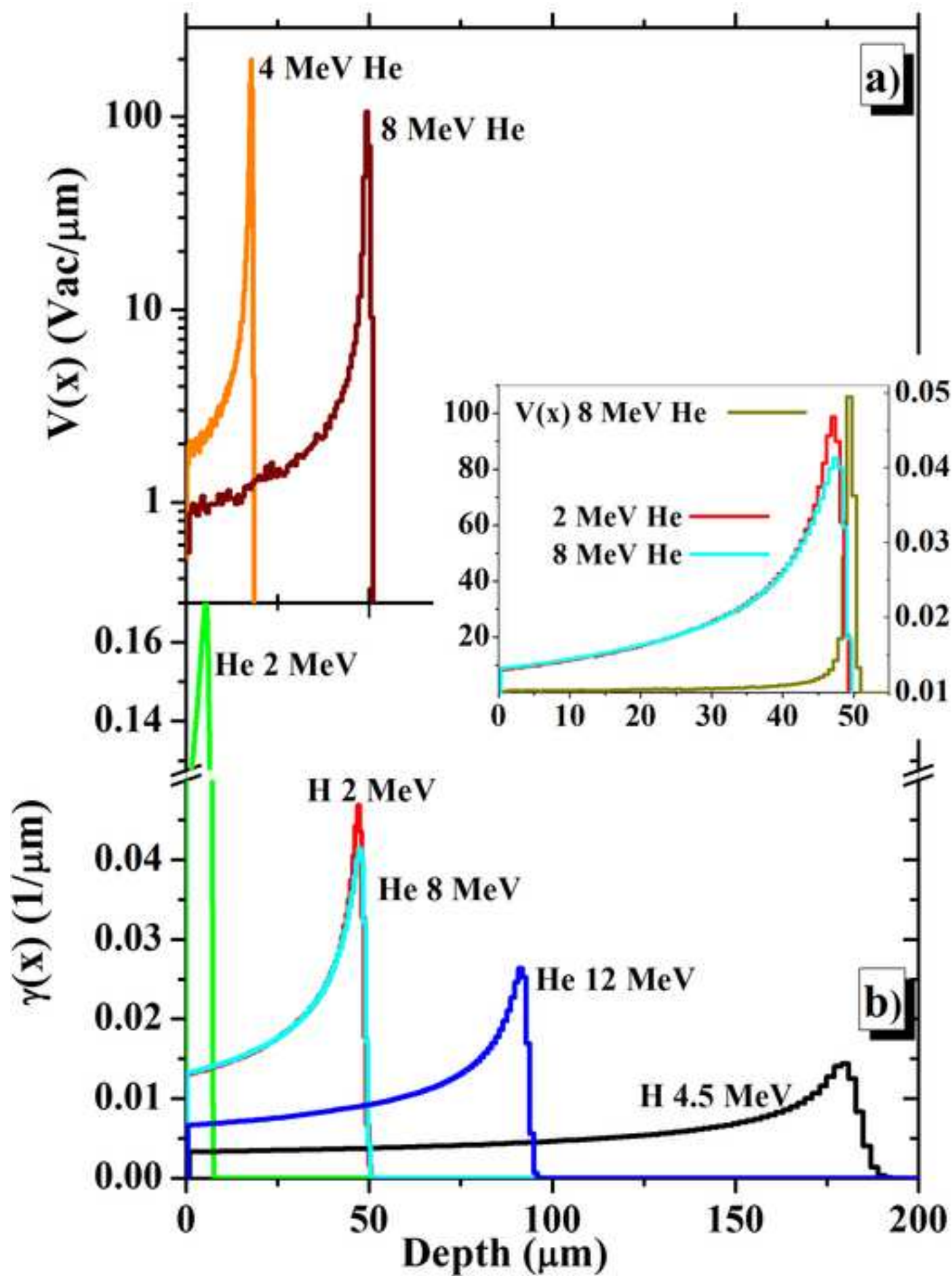


Figure6

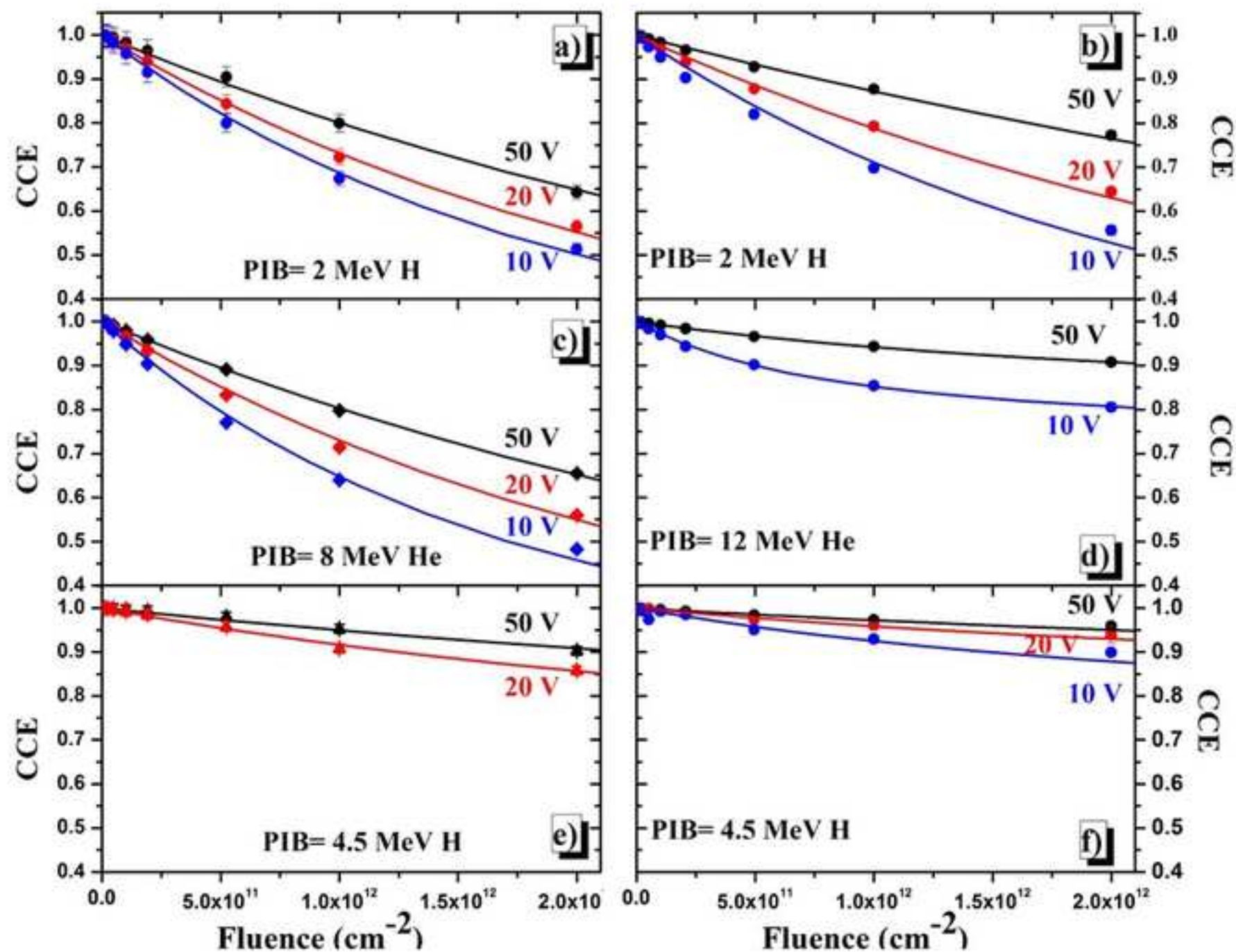




Figure7

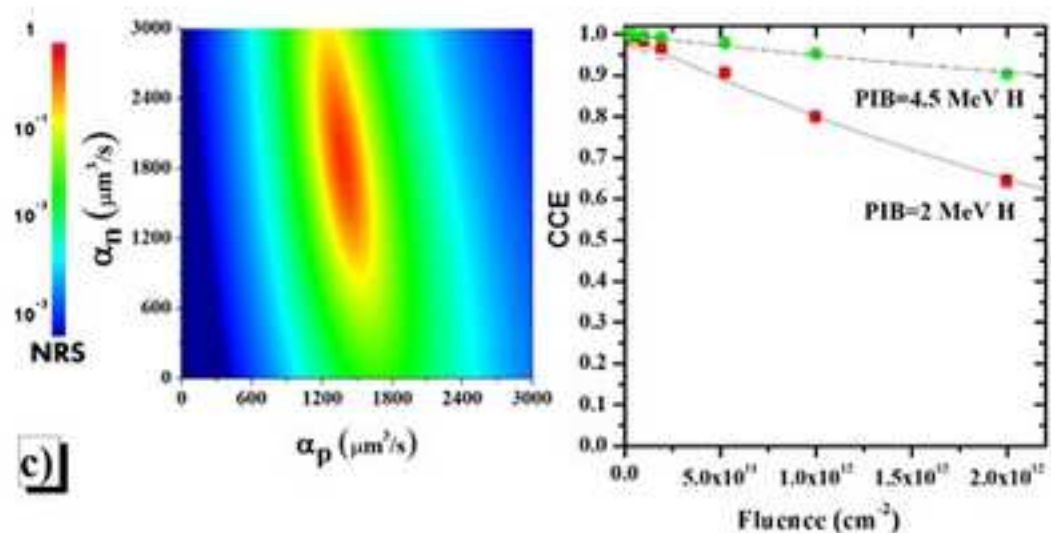
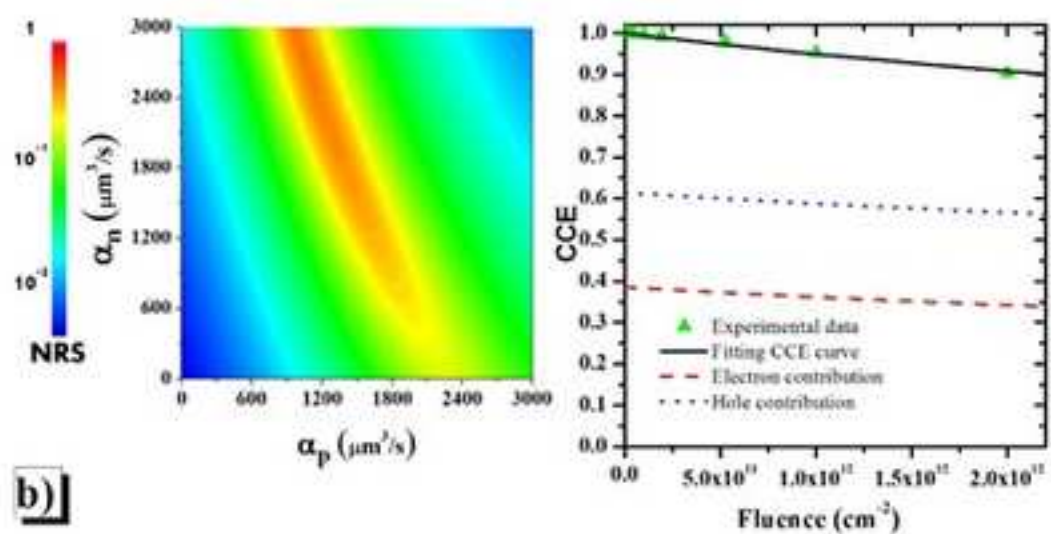
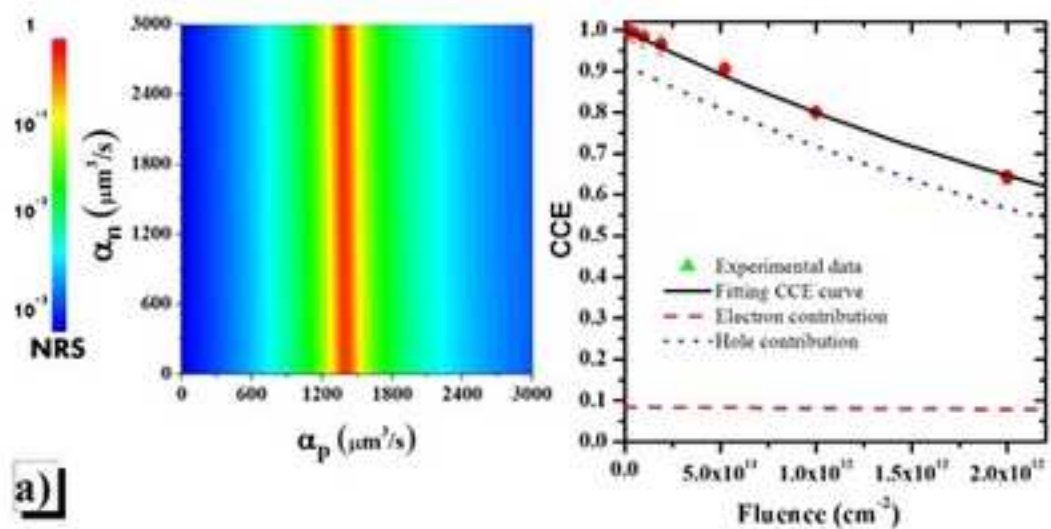


Figure8

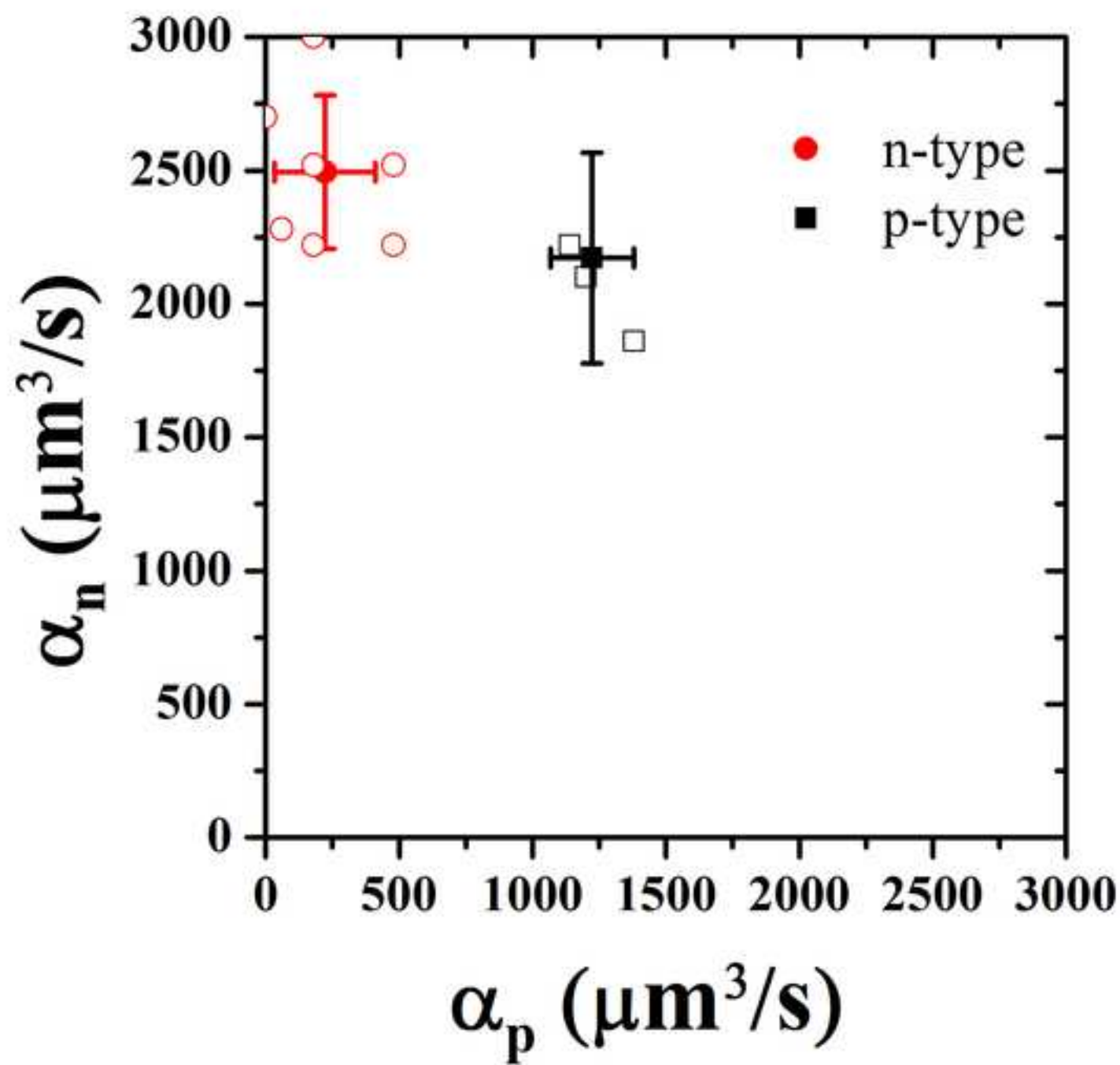


Figure9

